Anchoring Effect for Membrane-Confined Liquid Crystal System

Doctor thesis

Anchoring Effect for Membrane-Confined Liquid Crystal System
(膜に閉じ込められた液晶系に対するアンカリングの効果)

Shun Okushima

H.28

ABSTRACT

Introduction

Liquid crystal (LC) phases have ordering in the molecular directions but with a lack of some orders in the molecular positions. Due to the orientation ordering, the LC materials show elasticity. At an interface, there appears a coupling between the orientation order of the LC and the interfacial normal, which is called "anchoring". Such a coupling is the main target of the present thesis. Even if the LC in the bulk phase is in an isotropic phase, the LC within a narrow layer near the interface can show an orientation order due to the anchoring. In this case, interesting interfacial behaviors are expected to be observed originating from the different orders between the region near the interface and the bulk region.

Utilizing the surface anchoring effect in the molecular detection technique is one of the promising applications, where the LC orientation by the anchoring gives information about an existence of a target molecule. If the interface is flexible, it can change its shape so that more information on the target molecules can be obtained. Thus, it is important to accumulate knowledge on the relation between the anchoring behavior and the shape of the interface. For example, when the interface can deform, mechanical properties of the interface such as the interfacial tension and the bending rigidity have noticeable effects.

Method

For simplicity, we study a thin LC layer floating in a simple isotropic fluid, where the interfaces are covered by surfactant layers. To estimate the interfacial properties theoretically, we performed a molecular simulation using a coarse-grained molecular model based on Monte-Carlo (MC) method. Our model is composed of three types of molecules, i.e. the ellipsoidal molecules as the LC, spherical molecules that form a simple isotropic liquid surrounding the LC layer, and the surfactant molecules that form assembled molecular layer between the LC phase and the simple liquid. In a single surfactant molecule, a particle at one chain end corresponds to a hydrophilic particle which attractively interacts with the simple fluid, and the other particles correspond to hydrophobic particles which interact attractively with the LC particles. Confining the LC layer by the surfactant membranes, the interface becomes stable.

The strength of the anchoring effect is expressed by an anchoring param-

eter ξ, where ξ describes the anisotropy of the potential depth. For the case with $\xi = 1$, the interaction between the LC and the surfactant is orientationally isotropic, and therefore no anchoring interaction is effective. On the other hand, the anchoring is called " homeotropic anchoring " when $\xi > 1$, where the LC director $\boldsymbol{n}$ tends to be parallel to the interfacial normal vector $\boldsymbol{k}$.

Results

(i) Results of Monte-Carlo simulation

From the MC simulations, we obtained several results. First, we observed a decrease in the interfacial tension when ξ is increased. Second, we found a change in the tendency of the bending rigidity at a certain $\xi = \xi_{\mathrm{m}}$ and simultaneously a change in the orientational order of the LC material near the interface. All of these features can be explained by the anchoring effect which gives a homeotropic anchoring for $\xi > 1$.

Since the molecular orientation is fluctuating thermally, the interaction energy between the LC and the membrane by the anchoring also fluctuates. The energy fluctuation increases when the anchoring strength increases. Such an energy fluctuation induces a fluctuation of the area of the membrane because the equilibrium area of the membrane is dependent on the interaction energy. Then, the fluctuation of the area of the membrane becomes larger by increasing ξ, resulting in a decrease in the interfacial tension.

As was discussed above, the energy fluctuation is due to the ordering of the LC near the interface. When $\xi > 1$, the LC orientation averaged over the interfacial region is directed to the interfacial normal direction due to the anchoring. In this case, the LC near the interface has a directional order on the average. Such an orientation direction induced by the anchoring does not in general coincide with the natural direction of the LC determined by its elasticity. Then the local LC directions near the interface are determined by the competition between the contribution of the LC elasticity and that of the anchoring, which leads to a renormalization of the effective bending rigidity. Such a competition leads to two different regimes in the anchoring strength divided at a certain threshold value $\xi = \xi_{\mathrm{m}}$.

When the anchoring effect is small compared to the LC elasticity, i.e. $1 < \xi < \xi_{\mathrm{m}}$, the local LC director near the interface does not fit to the local membrane normal due to the LC elasticity, which avoids a spatial variation of the LC directors. As a result, most of the LC directors are oriented

to the same direction, i.e. the *average* normal direction of the membrane. In this case, when the membrane fluctuates, the mismatch between the local membrane normal and the LC director imposes a penalty for the deformation of the membrane, resulting in an increase in the effective bending rigidity.

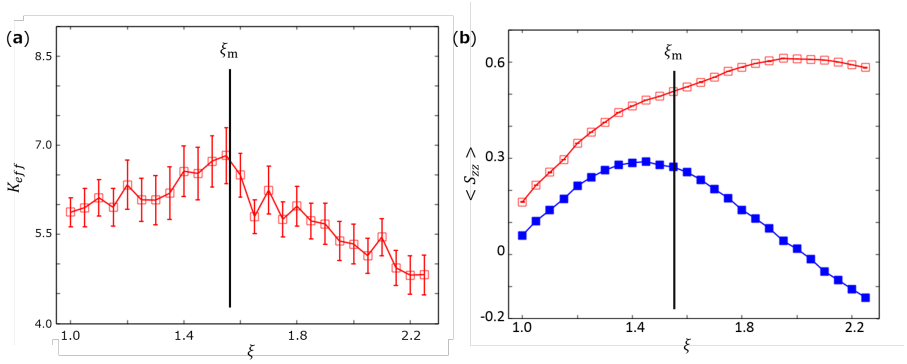

Fig. 1: The bending rigidity (a) and the LC orientational order near the interface (b). Both quantities are the functions of ξ. In graph (b), the blue curve corresponds to the LC order just at the interface.

Contrary to the above weak anchoring case, the behavior changes when $\xi > \xi_{\rm m}$, i.e. a strong anchoring case. In this case, the bending rigidity changes its dependence on ξ from increasing to decreasing behaviors. If the effect of the homeotropic anchoring is strong enough, the LC directors near the membrane tend to orient to the local membrane normal. Then, the LC orientation near the interface is distorted when the membrane fluctuates, which leads to an increase in the penalty due to the LC elasticity. To suppress this elastic penalty of LC, the LC molecules just at the interface, where the LC molecules have a contact with the surfactant on the membrane, change its direction from the average membrane normal to the lateral direction along the membrane. In this case, when the membrane fluctuates in the direction perpendicular to the LC orientation in the lateral plane, the LC elastic penalty is not imposed, and the bending rigidity of the membrane effectively decreases. Such a change in the LC orientation from the membrane normal to the lateral direction of the membrane is realized by the so-called " depletion effect " which originates from the entropic effect with respect to the steric hindrance on the translation of the LC molecules just at the interface. The change in the LC orientation just at the interface is confirmed by

the orientation order parameter of the LC near the membrane which shows the similar behavior to the bending rigidity, that is, the order changes its tendency from increasing to decreasing behavior (See Fig.1). Note that the LC molecules slightly away from the membrane (but near the interface) retain the orientation in the membrane normal by the anchoring interaction realized by the parameter ξ. Then the effect of the anchoring remains so that the total interaction energy is advantageous although the LC orientations are mixed (the membrane normal and the lateral orientation) near the interface.

(ii) Results of fitting using continuum model

These results have been explained by using a continuum model of the LC order and the membrane shape, where the model includes some additional effects, i.e. the effect of anchoring, the correlation between the fluctuation in the LC orientation and the fluctuation in the membrane shape, and the effect of the LC ordered layer. Then we obtained the information of these effects by fitting the continuum model to our simulation results. Performing similar simulations for some values of the LC parameters and fitting the results, we can obtain the dependency of the additional effects of the continuum model to the LC material parameters. These analysis offers us a way to determine the properties and the deformation of the interface that confines the LC material. We will be able to apply such model system to, for example, a molecular sensor.

Contents

Symbol List

——————— Chapter2 ———————

$\boldsymbol{r}_{ij} = \boldsymbol{r}_i - \boldsymbol{r}_j$: relative position vector between i at $\boldsymbol{r}_i$ and j at $\boldsymbol{r}_j$ particles
$r_{ij} = |\boldsymbol{r}_{ij}|$: distance between i and j particles
$\hat{\boldsymbol{r}}_{ij} = \boldsymbol{r}_{ij}/r_{ij}$: relative azimuthal vector between i and j particles
$\hat{\boldsymbol{u}}_i$: molecular axis vector of i's liquid crystal molecule
ϵ_0 : energy unit
σ_0 : length unit
ϵ_{ij} : energy depth of potentials between i and j particles
σ_{ij} : distance between two particles when they contact at their surface
(it expresses diameter of i's particle when $i = j$)
κ : aspect ratio of an ellipsoidal particle as a liquid crystal molecule
κ' : energy depth ratio for liquid crystal molecules of end-to-end to side-by-side configurations
χ : GB parameter as a function of κ
χ' : GB parameter as a function of κ'
μ, ν : GB parameters which determine the effects of κ and κ' for GB potential
k_{spring} : energy constant (spring constant) of harmonic spring potential
k_{bend} : energy constant of beding potential working on surfactant molecule
ξ : anchoring parameter
χ'_{sg} : parameter with respect to potential between LC molecule and spherical particle as a function of ξ
k_{B} : Boltzmann constant
T : temperature of simulation system
T_{r} : room temperature (basis of temperature in our simulation)
P : pressusre imposing on simulation system
N : the number of particles
N_{s} : the number of surfactant molecules
N_{l} : the number of liquid crystal molecules
N_{w} : the number of hydrophilic particles

———————————————————

——————— Chapter3 ———————

γ_{eff} : effective interfacial tension of membrane, that is,
it includes effects of surrounding liquids of membrane
K_{eff} : effective bending rigidity of membrane
$\boldsymbol{q} = (q_x, q_y)$: wave vector relative to plane (x, y) in cartesian coordinates
$q = |\boldsymbol{q}|$: absolute value of wave vector $\boldsymbol{q}$

$h(x, y)$: z coordinate of membrane at (x, y) in cartesian coordinates
(it expresses shape of membrane)
$h(\boldsymbol{q}), h_{\boldsymbol{q}}$: Fourier component of $h(x, y)$
A_{m} : area of membrane
l_{m} : distance between two membrane (thickness of liquid crystal thin layer)
$\boldsymbol{Q}(\boldsymbol{r})$: tensor order parameter of liquid crystal at $\boldsymbol{r}$
$S(\boldsymbol{r})$: scalar order parameter of liquid crystal which is
derived as the maximum eigenvalue of $\boldsymbol{Q}(\boldsymbol{r})$ in nematic phase
$\boldsymbol{n}(\boldsymbol{r})$: director of liquid crystal at $\boldsymbol{r}$ which is the local average of molecular orientations
L_α : size of system in α-direction
a_α : size of cell in α-direction which is used for definition of volume fraction at $\boldsymbol{r}$
b_α : the number of cells

f_0 : local free energy density with respect to ordering of liquid crystal
f_{el} : elastic energy density of liquid crystal
H : mean curvature of membrane
$A(T), B, C$: coefficients of local ordered energies in free energy of liquid crystal
L_2 : elastic constant in free energy of liquid crystal
γ : interfacial tension of membrane
K : bending rigidity of membrane
γ_{a} : anchoring strength in continuum model
K_{a} : coefficient corresponding to fluctuational coupling between liquid crystal and membrane
K_{b} : effect of nematicl layer
$\boldsymbol{R}$: position vector of fragment on membrane
$\boldsymbol{g}_\alpha$: coordinate vector in α-direction in curvilinear coordinates on membrane
($\alpha = 1, 2$ correspond to tangential direction and $\alpha = 3$ to normal one)
$m_{\alpha\beta} = \boldsymbol{g}_\alpha \cdot \boldsymbol{g}_\beta, (\alpha = 1, 2)$: metric tensor on membrane
$\sqrt{d_g}$: area fragment of membrane where $d_g = \det |m_{\alpha\beta}|$
$f_{\alpha\beta} = (\partial \boldsymbol{g}_\alpha / \partial x_\beta) \cdot \boldsymbol{g}_3$: second fundamental form
m_α : component of normal vector $\boldsymbol{m}$ on membrane

---

Chapter 1

Introduction

1.1 Introduction to liquid crystals

1.1.1 Orientational order of liquid crystal

Many materials composed of atoms or molecules experience phase transitions by changing temperature, pressure, and other control parameters. For example, by increasing temperature, a material shows a phase transition from initial solid phase to liquid phase at melting temperature. In gas and liquid phases, materials have a perfect symmetry, that is, continuous symmetry for translation and rotation. On the other hand, in solid phase composed of molecules, a certain symmetry is broken, for example when the translational symmetry is broken, a lattice structure emerges for molecular position. A solid composed of molecules frequently shows a molecular orientational order in the case that the molecule has an anisotropic shape. When a molecule has an orientational order in a lattice structure at low temperature, a positional melting can happen when only the translational degrees of freedom are released while the direction order is present, resulting in a fluid phase with the molecular orientatioal order even in the equilibrium state. Such a fluid phase with molecular orientational order is called "liquid crystal", and is abbreviated as LC[1,2]. This phase shows both solid-like properties with respect to the orientational order and liquid-like ones due to the disordered state of the molecular positions. The materials that shows LC phases by changing the temperature are called "thermotropic liquid crystals". On the other hand "lyotropic liquid crystals" mean materials that show LC phase (in a broad sense) depending on their concentration or density. They are,

for example, surfactants, lipids, and block-copolymers, and form various ordered structures, such as micelles, cylinders, planar lamellae, or vesicles. In this thesis we focus on the properties of both types of LC. Hereafter we restrict the arguments on the thermotropic LC that have rod-like shapes. Since

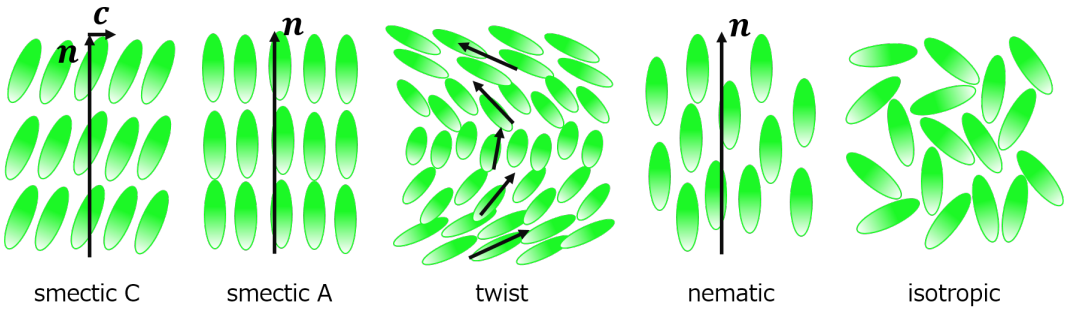

Fig. 1.1: LC phases.

the material showing LC phase is frequently called LC material (and such a molecule is also), we will use the word "LC" as the meaning of the LC phase unless noted explicitly. "Nematic" phase that is one of the LC phases has a long range molecular orientational order and has no long range positional order. A case with one dimensional positional order but without positional order in the vertical directions in an LC phase results in a layered structure with orientational order, which is called "smectic" phase. Such a smectic phase is further classified according to the nature of the orientational order beetween layers; when molecules are directed to the layer normal direction, it is called "smectic A" phase, and when it is tilted to the layer normal, it is called "smectic C". Many other complex ordered phases have been observed, especially in a case of chiral molecule which shows "cholesteric" or "twist nematic" phase where uniaxially oriented 2-dimensional planes are twisted in the direction normal to the plane. In materials that show LC phases, the temperature where the phase changes from LC phase to a perfectly-symmetric liquid is called clearing temperature. In the symmetric phase, the material is clear so that an incident light can transmit through it. At the melting temperature, these materials remain orientational order or a specal orientation direction which largely fluctuates spatially and temporally although they lose the periodic arrangement of the molecular positions. Then an incident light is scattered into various directions, resulting in an opaque state.

The structures and behaviors of an LC phase can be described in a similar manner as a colloidal system is described in terms of the density distribution function, which is performed by Onsager [3]. He assumed that (i) an LC molecule is a rod-like rigid body, (ii) the volume fraction of LC molecules is much smaller than 1, and (iii) the length of the rod is much longer than its width. Here, we start to consider a system including spherical colloids, subsequently extend a system with an orientational anisotropy in the particles. The partition function of the spherical colloidal system interacting through a potential $u_{i,j}$ is given by

$$H = \frac{1}{2m}\sum_i \boldsymbol{p}_i^2 + \sum_{i<j} u_{i,j}, \tag{1.1}$$

$$Z = \frac{1}{N!h^{3N}}\int\cdots\int \exp\left(-\beta H\right) d^{3N}q d^{3N}p = \frac{1}{N!\Lambda^{3N}} Q_N, \tag{1.2}$$

$$Q_N = \int\cdots\int \exp\left(-\beta\sum_{i<j} u_{i,j}\right) d^{3N}q, \tag{1.3}$$

$$\Lambda = h/\sqrt{(2\pi m k_{\mathrm{B}} T)}, \tag{1.4}$$

where m is the mass of the particle, $\boldsymbol{p}_i$ is the momentum of i'th particle, h is Planck constant, k_{B} is Boltzmann constant, T is temperature, and N is the total number of particles in the system. Λ is thermal de Broglie wave length. Then a free energy of this spherical particle system is given as

$$\frac{F}{Nk_{\mathrm{B}}T} = -\frac{1}{N}\ln Z = \ln\left(\Lambda^3\rho\right) - 1 + B_2\rho, \tag{1.5}$$

$$\Phi_{i,j} = \exp\left(-\beta u_{i,j}\right) - 1, \tag{1.6}$$

$$B_2 = -12V\int\int \Phi_{i,j} d^3q_i d^3p_i, \tag{1.7}$$

where $\rho = N/V$ is the material density, and V is the system volume. It is assumed that $|u_{i,j}| \ll k_{\mathrm{B}}T$ and therefore $|\Phi_{i,j}| \ll 1$ and $|B_2| \ll V$. In deriving Eq.1.5, Stirling's approximation $\ln N! \approx N\ln N - N$ was used assuming $N \gg 1$.

Next, let us consider that the particle has an orientatoinal probability distribution $f_{\boldsymbol{u}}(\Omega)$ where $\boldsymbol{u}$ is the unit vector which expresses the molecular orientatoin direction and Ω is the solid angle. $f_{\boldsymbol{u}}(\Omega)$ satisfies the normalization condition $\int f_{\boldsymbol{u}}(\Omega)d\Omega = 1$. For simplicity, it is assumed that the

degrees of freedom of position and momentum of the particle are independent of its orientation, so that the number of particles observed in a volume element at $\boldsymbol{u}$ is $\rho_{\boldsymbol{u}}(\boldsymbol{r})d\Omega = \rho f_{\boldsymbol{u}}(\Omega)d\Omega$. The 2-body interaction is given by $\int_{\Omega'} B_{2,\boldsymbol{u}}(\Omega,\Omega')\rho f_{\boldsymbol{u}'}(\Omega')d\Omega'$ which expresses the interaction energy integrated over all possible orientations $f_{\boldsymbol{u}'}(\Omega')$. Then we can get $\tilde{F}_{\boldsymbol{u}}(\Omega)$ by inserting the above expressions into Eq.1.5, assuming that the all initial colloid particles have the director $\boldsymbol{u}$ following the distribution function $f_{\boldsymbol{u}}(\Omega)$. Therefore total free energy can be obtained by integrating $F_{\boldsymbol{u}}(\Omega)$ over Ω under the probability weight defined by the orientational distribution $f_{\boldsymbol{u}}(\Omega)$ as follows,

$$\begin{aligned}\frac{F_{\text{aniso}}}{Nk_{\text{B}}T} =& \frac{1}{Nk_{\text{B}}T}\int_{\Omega} f_{\boldsymbol{u}}(\Omega)\tilde{F}_{\boldsymbol{u}}(\Omega)d\Omega \\ =& \left\{\ln\left(\Lambda^3\rho\right)-1\right\} + \int_{\Omega} f_{\boldsymbol{u}}(\Omega)\ln\left(4\pi f_{\boldsymbol{u}}(\Omega)\right)d\Omega \\ &+ \rho\int_{\Omega}\int_{\Omega'} B_{2,\boldsymbol{u}}(\Omega,\Omega')f_{\boldsymbol{u}}(\Omega)f_{\boldsymbol{u}'}(\Omega')d\Omega d\Omega'. \end{aligned} \tag{1.8}$$

In Eq.(1.8), the first term is the free energy of an isotropic system, the second term means the orientational entropy, and the third term is the orientation-dependent 2-body interaction. Note that in above calculation the higher order terms in $\Phi_{i,j}$ are neglected. Onsager justified this approximation by considering only the excluded volume interaction between two anisotropic particles with a uniaxial shape. Then, he assumed that $B_{2,\boldsymbol{u}}(\Omega,\Omega') = L^2D|\sin\gamma|$ where L and D are the length of the long axis and the width of the molecule, and γ is an angle between the directions of two interacting molecules. To obtain the most probable distribution function $f^*_{\boldsymbol{u}}(\Omega)$, Eq.(1.8) is minimized under the normalization condition $\int f^*_{\boldsymbol{u}}(\Omega)d\Omega = 1 \rightarrow \frac{\delta F_{\text{aniso}}}{Nk_{\text{B}}T} + \lambda\int \delta f^*_{\boldsymbol{u}}(\Omega)d\Omega = 0$ where λ is the Lagrange multiplier. The resulted equation is difficult to solve due to its non-linearity. Onsager introduced a trial function as the orientational distribution function $f_{\boldsymbol{u}}(\Omega) = C\cosh\left(\eta\cos\theta\right)$ where C is a constant for the normalization constraint for $f_{\boldsymbol{u}}(\Omega)$ and η is a parameter, and solved the minimization problem with respect to η. This minimization, however, leads to an unrealistic behavior of the LC phase.

Maier and Saupe used a molecule with only one symmetric axis in a heat bath [4]. They started to construct a Gibbs free energy including an interaction energy depending on the orientational order parameter,

$$G^*(p,T) = G^*_0(p,T) + \int f_{\boldsymbol{u}}(\Omega)\ln\left(4\pi f_{\boldsymbol{u}}(\Omega)\right)d\Omega + G^*_s(p,T,S), \tag{1.9}$$

where $G^*(p,T) = G(p,T)/(Nk_{\rm B}T)$ is the dimensionless Gibbs free energy per single particle and other values $(\cdot)^*$ have the same mean. $G_s^*(p,T,S)$ is the effective 2-body interaction energy as a function of the order parameter S defined as

$$S = \int f_{\boldsymbol{u}}(\Omega)\frac{1}{2}(3\cos^2\theta - 1)d\Omega. \tag{1.10}$$

Then, $G_s^*(p,T,S)$ is given by

$$G_s^*(p,T,S) = -\frac{1}{2}u^*(p,T)S^2, \tag{1.11}$$

where $u^*(p,T) > 0$ is a (dimensionless) intermolecular interaction potential per single particle. The distribution function that minimizes the Gibbs energy Eq.1.9 is obtained under the constraint from the normalization condition $\int f_{\boldsymbol{u}}(\Omega)d\Omega = 1$,

$$f_{\boldsymbol{u}}(\theta) = \frac{1}{4\pi Z}\exp\left(m^*\cos^2\theta\right) \text{ and } Z = \int_0^1 \exp\left(m^*x^2\right)dx, \tag{1.12}$$

where $m^* = 3u^*S/2$. Then a self consistent equation for the order parameter S is obtained from Eq.(1.10) using the distribution Eq.1.12. The resulting threshold value of the order parameter at the nematic-isotropic transition temperature $T_{\rm c}$ agrees with the experimental results.

In the vicinity of the transition temperature, considering that the order parameter with respect to the orientation of the LC material is small, the free energy density can be expanded in a power series as follows;

$$f = \frac{1}{2}A(T)Q_{\alpha\beta}Q_{\alpha\beta} + \frac{1}{3}BQ_{\alpha\beta}Q_{\beta\gamma}Q_{\gamma\alpha} + \frac{1}{4}C\left(Q_{\alpha\beta}Q_{\alpha\beta}\right)^2 + f_{\rm el}, \tag{1.13}$$

$$f_{\rm el} = \frac{1}{2}L_1\nabla_\alpha Q_{\alpha\gamma}\nabla_\beta Q_{\beta\gamma} + \frac{1}{2}L_2\nabla_\alpha Q_{\beta\gamma}\nabla_\alpha Q_{\beta\gamma} + \frac{1}{2}L_3 Q_{\alpha\beta}\nabla_\alpha Q_{\gamma\delta}\nabla_\beta Q_{\gamma\delta}, \tag{1.14}$$

where $Q_{\alpha\beta}$ is a symmetric and trace-less 2-rank tensor defined using the orientation of LC. In Eqs.1.13 and 1.14, some possible terms for combinations of indices of ∇_α or $Q_{\alpha\beta}$, and interactions with external field are omitted for simplicity. In a microscopic description of LC phase, the orientational order is realized by the interaction between LC molecules, which defines a characteristic length scale $k_{\rm LC}$ of the elastic interaction. $Q_{\alpha\beta}$ is the averaged value of the molecular orientation whithin the length scale $k_{\rm LC}$, usually defined as

$Q_{\alpha\beta} = \langle u_\alpha u_\beta - \delta_{\alpha\beta}/3 \rangle$ where u_α is the α-component of unit vector along the molecular long axis. Each term in Eq.(1.13) means the local "orientational" energy, and the term $f_{\rm el}$ is the short range elastic interaction over the characterictic length $k_{\rm LC}$ of the molecular orientation. Equation 1.13 is then a continuum model for LC and called Landau-de Gennes free energy density [5], which is basically the Taylor expansion of the Maier-Saupe type free energy for small $u^*(p,T)$ in Eq.1.12 with the tensor form for the order parameter.

The expansion of the Maier-Saupe type free energy is for spatially uniform systems. Spatial non-uniformity can be taken into account in the Landau-de Gennes free energy by assuming a local equilibrium, where one can describe an inhomogeneous structure for the orientational field. When the LC has a uniaxial orientation averagely, i.e. the case where the degree of the orientational order is homogeneous in the whole system, the tensor order parameter $Q_{\alpha\beta}$ is written as

$$Q_{\alpha\beta} = 2S(n_\alpha n_\beta - \frac{1}{2}\delta_{\alpha\beta}), \text{ in 2D}, \tag{1.15}$$

$$Q_{\alpha\beta} = \frac{3}{2}S(n_\alpha n_\beta - \frac{1}{3}\delta_{\alpha\beta}), \text{ in 3D}, \tag{1.16}$$

where S is a scalar order parameter of LC (generally depends on the coordinates of space variable), n_α the α-component of the director vector which means the local averaged-orientational vector of the uniaxial nematic, and $\delta_{\alpha\beta}$ is the unit tensor. By assuming constant S in Eq.(1.16), the important terms in the free energy density Eq.(1.13) lead to the following form:

$$f = \frac{1}{2}K_1(\boldsymbol{\nabla}\cdot\boldsymbol{n})^2 + \frac{1}{2}K_2(\boldsymbol{\nabla}\cdot(\boldsymbol{\nabla}\times\boldsymbol{n}))^2 + \frac{1}{2}K_3|\boldsymbol{n}\times(\boldsymbol{\nabla}\times\boldsymbol{n})|^2, \tag{1.17}$$

where

$$K_1 = \frac{9}{4}S^2\left(L_1 + 2L_2 - L_3S\right), \tag{1.18}$$

$$K_2 = \frac{9}{4}S^2\left(2L_2 + L_3S\right), \tag{1.19}$$

$$K_3 = \frac{9}{4}S^2\left(L_1 + 2L_2 + 2L_3S\right). \tag{1.20}$$

This form of the free energy density describes the distortion energy of the uniaxial nematic system, and is called Frank elastic energy [6]. Three rep-

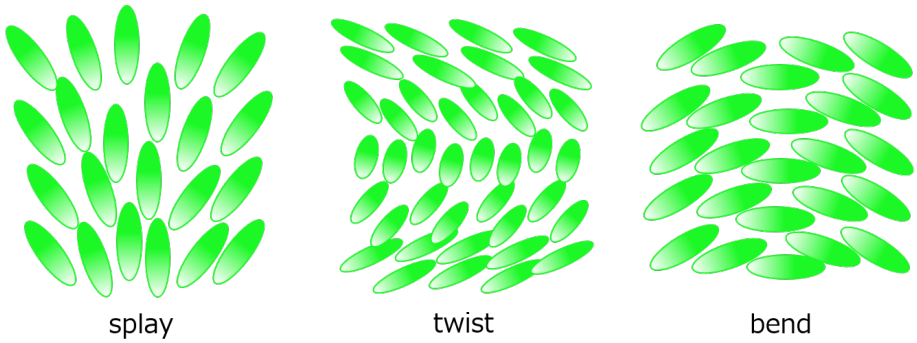

Fig. 1.2: LC configurations.

resentative coefficients mean "splay" (K_1), "twist" (K_2), and "bend" (K_3) configurations, and other surface terms or their coefficients are omitted for simplicity. This Frank elastic energy is useful in describing the systems free from defects a large deformation for the director field. We will use, in the following sections, Landau-de Gennes type free energy because our system is an inhomogeneous one that includes some boundaries or orientational defects.

1.1.2 Boundary condition for LC

At the boundary surface of a real system, the LC molecules interact with the surface-constructing molecules and also with the material outside the surface. Due to such an interaction, the directors of LC molecules are "directed" to a certain direction at a boundary. This effect is called "anchoring". When the characteristic anchoring energy (W_a) is much larger than the elastic energy of LC ($W_a \gg K$: K is the averaged elastic constant), the director at the surface is fixed because of the anchoring potential that realizes a certain orientation. In this case, the surface free energy no longer contributes to the total energy because the surface energy is just a constant. On the other hand, when $W_a \leq K$, the surface alignment is determined so that the total free energy including the surface energy is minimized. Thus, the achoring effect can be characterized by the length scale $b = K/W_a$, which is called "extrapolation length", where $b \approx 0$ corresponds to strong anchoring and $b \geq 1$ to weak anchoring. The anchoring leads to an anisotropic surface tension of the LC system which depends on the orientation of LC molecules at the surface. In simple liquids, the surface tension is determined microscopically from the

balance between the attractive and the repulsive interactions, which is called excess energy. In such a simple liquid case, the surface tension affects the extension of the surface area. In the case of LC surface, on the other hand, the LC molecules additionally affect the surface direction through the anchoring effect.

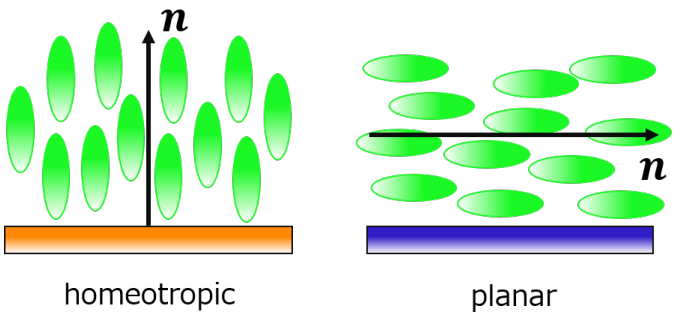

Fig. 1.3: Anchoring conditions.

In simple liquids or solids, the surface effects do not seriously affect the bulk properties due to no penalty for the deformation in simple liquids or very small thermal deformations in solids. However, in LC phase, due to its elastic energy which is comparable to the thermal energy, the deformation of the LC director field gives rise to an extra-free energy in the bulk region induced by the surface energy. Such an effect gives differect energies depending on the geometries of the surface by the anchoring. For the surface events at the LC surface, the important thing is not only the configuration of the director field but also that of the surface.

The anchoring is originating from the van der Waals force, the electric interaction between the ionic charges or the permanent dipoles, and steric interaction due to surface geometries. A "homeotropic" anchoring condition corresponds to a situation where the equilibrium LC director at the interface tends to direct parallel to the interfacial normal direction, while a "homogeneous" or "planar" anchoring condition is that the director points the tangential of the interface in the equilibrium state. In this thesis, we will mainly focus on the van der Waals force (including the anisotropic force) and the effects of the surface geometry, and on the homeotropic anchoring condition unless stated explicitly. When LC molecules are confined between two planar rigid plates, the behavior of the director field which is affected

by the anchoring is described in a manner already mensioned above. However, the order of orientation of LC is complicated. The LC order shows

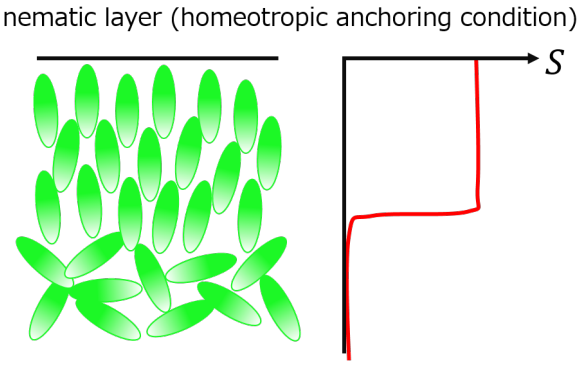

Fig. 1.4: Nematic layer.

pretransitional effects because it shows the first order transition due to the symmetrical difference reason between the isotropic and the (nematic) LC phase. Due to the pretransitional effects, an attractive behavior at the surface, called nematic wetting [7-9], is expected. When the LC material shows the isotropic phase in the bulk and is enclosed in a cell with anchoring force at the wall, the ordered LC phase regions appear in the vicinity of the wall near the transition temperature T_c. The locally ordered regions grow when the temperature approaches T_c and form an ordered layer, which is called the nematic wetting layer. Otherwise in the case of the LC confined in a spherical container, the director field is deformed by the competition between the anchoring and the elastic energy [10-18].

1.1.3 Defect of orientation in LC

In a solid with crystalline order, when an inhomogenuity in the arrangement of the atoms or the molecules emerges, an absence of the particle at a lattice point or a deformed structure of the crystal due to the inhomogenuity are called "defect". The structure arround the defect has a higher energy and cannot further deform due to the rigidity of the crystal. In LC phase, however, the structure around the defect has lower energy than that in the solid, which is the same or about 10 times larger than the thermal energy. Then the director in the LC phase can fluctuate and can be controlled in terms of the defect structure. A typical defect in LC phase is an orientational defect

that is called "disclination". When we trace the orientational change in the director field around a point, we may see an inconsistency about the LC orientation characterized by m which is either an integer or a half integer. This is described in polar coordinates as follows,

$$\theta(\varphi = 2\pi) - \theta(\varphi = 0) = \oint_0^{2\pi} \frac{d\theta}{d\varphi} d\varphi = 2\pi m, \tag{1.21}$$

$$m \equiv \frac{d\theta}{d\varphi}, \tag{1.22}$$

where θ is the angle of the director of the LC component in the polar coordinates and φ the coordinate about the azimuthal angle. In this case, the point where m is defined is the origin of the coordinates. When $m \neq 0$, the point corresponds to the orientational defect, disclination. m expresses the strength of the disclination. A point and a line disclination is known as types of the disclination. The line disclination is a continuously arranged structure like a one-dimensional array of the point disclination. Seeing the cross-section of the line disclination or rotating the plane in the symmetry axis of the director field, one can observe the point disclination. The elastic energy is stored around such disclinations due to the gradient of the director field. At the center of the disclination core, the orientational order is vanishing due to the large elastic energy of the orientational singularity. In this case, the strength of the disclination is defined in the region far from the disclination core.

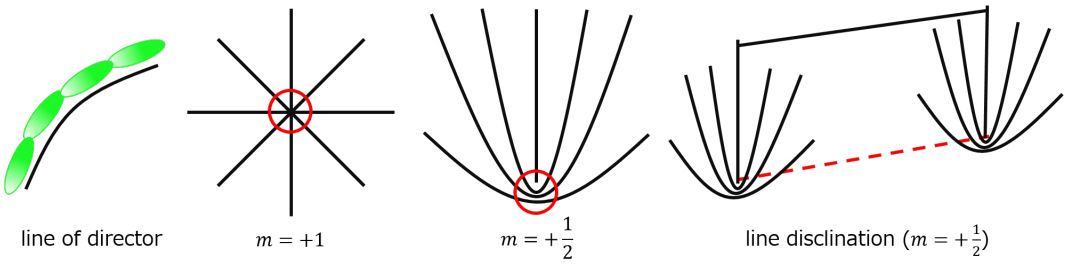

Fig. 1.5: Point and line disclinations.

A disclination can fluctuate or move by the following reasons. I) When a disclination is the line type, the line tension is worked along it due to the stored orientational elastic energy [19,20]. Then the length of the line disclination tends to be shorter due to the line tension. II) Because of a topological constraint on the rotation of the director field around a disclination,

the disclination cannot dissappear spontaneously in the equilibrium state. However, when two disclinations with the same strength $|m|$ but with different signs are close together whithin a characteristic length scale of the elastic energy, they approach each other and finally disappear [21,22,23]. Above two mechanisms result in the fluctuation of the disclination and the surrounding director field. The disclination can move by rotating or flowing the director field or the LC molecules, and the director rotation and flow couple each other [24]. Then the coupling affects the dynamics of the disclinations [25,26,27]. These properties of the defect of LC phase attract our attention and applications of the structured disclination are proposed, for example a particle trap [28,29].

1.2 Introduction of Membrane

1.2.1 Composition of membrane

Similarly to the thermotropic LC mentioned in section 1.1.1, the lyotropic LC forms some ordered fluid structures as equilibrium states [30]. In the case of lyotropic LC, molecules approach with each other when the relative concentration in mixture increases due to the specific interaction between the molecular structure and the environments. The molecules showing lyotropic LC phase are, for example, surfactants, lipids, and block-copolymers as was mentioned before. These materials have an amphiphilic property and also have hydrophilic "head" which is usually a polar group or ionic interacting with polar molecules like water, and have hydrophobic "tail" which is composed of, for example, hydrocarbon chains. Therefore, the assembly of the lyotropic LC molecules has some boundaries characterized by the molecular structure and the environments. The self-assembled structures formed by these molecules are versatile, i.e. micelles, cylinders, lamellae, vesicles, or their buildings. Because of their amphiphilic property, water escapes from a region where the tail concentrates but favors a surface composed of the head groups. On the other hand, oily molecules favors the tail-concentrating region. The resulting structure in lyotropic LC phase depends on the concentration of the LC molecules in the solution. The concentration at which these molecules start to self-assemble is called critical micelle concentration (CMC), where the micellar structure is first formed. Above the CMC, the self-assembling larger structures are determined to minimize the surface area

and the curvature energy. These effects are respectively due to the surface tension and the curvature elasticity.

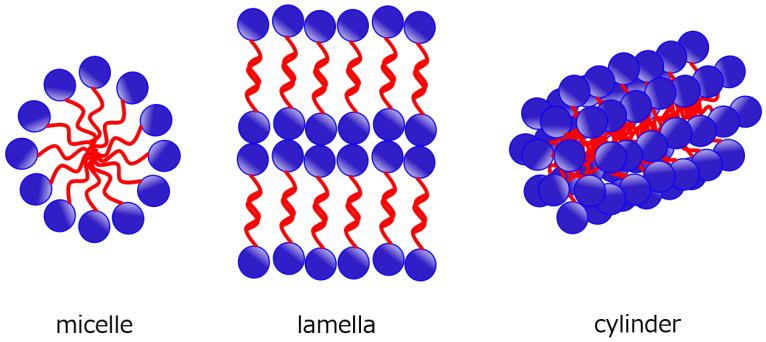

Fig. 1.6: Phases of surfactant.

Let us focus on a planar membrane that is a part of a lamella structure or a vesicle (only monolayer is considered hereafter) surface, composed of the surfactant molecules [31]. In such a membrane, the surfactant molecules are on the average directed to the membrane normal direction, and are thermally fluctuating. Due to the attractive interaction between surfactant molecules and due to their occupied area in the membrane determined by the repulsive interaction, the total area of the membrane tends to remain constant and the instantaneous deviation from the average area causes the surface tension. Since the surfactant molecules have the thread-like body with slight rigididy, the elastic interaction is worked on the membrane due to the similarity to the smectic single layer of the thermotropic LC material. The curvature of the membrane tends to be constant everywhere on the membrane, and the deviation causes the curvature elasticity. Therefore the geometry of the membrane surface is smooth, especially in the case of the membrane with larger area than the length as twice as the membrane thickness (about the length of the surfactant molecule).

1.2.2 Physical model of membrane

When the lateral dimension of the membrane is much larger than its thickness, one can regard the membrane as a thin curved surface and can describe it mathematically [32]. Let us define a position vector $\boldsymbol{R}$ on the membrane using a curvilinear coordinates $u = (u_1, u_2)$ (regarding the film

surface as 2D space). As the film and the position vector $\boldsymbol{R}$ are in the

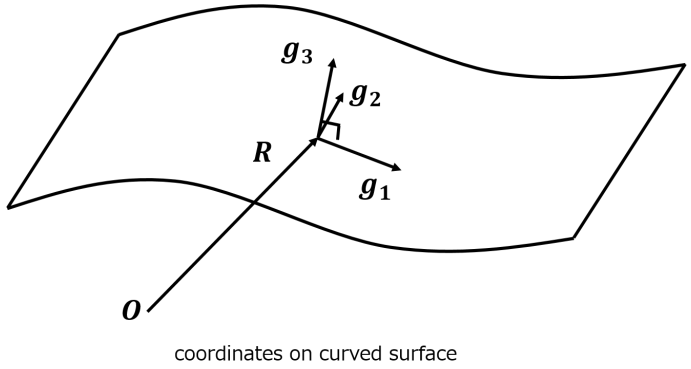

Fig. 1.7: Mathematical model of membrane.

3D space, the 3-characteristic orthogonal vectors on the film can be defined as $\boldsymbol{g}_\alpha = \partial \boldsymbol{R}/\partial u_\alpha (\alpha = 1, 2)$ are the tangential vectors along the coordinate axis u_α and $\boldsymbol{g}_3 = (\boldsymbol{g}_1 \times \boldsymbol{g}_2)/|\boldsymbol{g}_1 \times \boldsymbol{g}_2|$ which is the film normal vector. Here metric tensor $m_{\alpha\beta} \equiv \boldsymbol{g}_\alpha \cdot \boldsymbol{g}_\beta$ and $|\boldsymbol{g}_1 \times \boldsymbol{g}_2| = \sqrt{d_g}$ where $d_g = \det |m_{\alpha\beta}|$ is the metric defined as the determinant of $m_{\alpha\beta}$ ($d_g = \det |(m_{\alpha\beta})| = g_{1\eta} g_{1\eta} g_{2\nu} g_{2\nu} - g_{1\eta} g_{2\eta} g_{1\nu} g_{2\nu} = (\delta_{\eta'\eta}\delta_{\nu'\nu} - \delta_{\eta'\nu}\delta_{\nu'\eta}) g_{1\eta} g_{1\eta'} g_{2\nu} g_{2\nu'} = \epsilon_{\gamma\eta\nu}\epsilon_{\gamma\eta'\nu'} g_{1\eta} g_{1\eta'} g_{2\nu} g_{2\nu'} = |\boldsymbol{g}_1 \times \boldsymbol{g}_2|^2$). This metric d_g relates the coordinates system to the distance on it. Using $\boldsymbol{g}_1, \boldsymbol{g}_2$ and $\boldsymbol{g}_3$, the second fundamental form of the coordinates u on the membrane is defined as $f_{\alpha\beta} \equiv (\partial \boldsymbol{g}_\alpha/\partial u_\beta) \cdot \boldsymbol{g}_3$. According to this form, the more the film bends, the larger the component of the film normal in $\partial \boldsymbol{g}_\alpha/\partial u_\beta$ becomes. Since the absolute value of $f_{\alpha\beta}$ becomes larger in this case, $f_{\alpha\beta}$ can be related to the "curvature". Then the mean curvature of the film is defined as $H = f^\alpha_\alpha/2$, which is invariant under the rotation of the coordinates on the film. In this case, H is negative for a spherical or cylinderical film in the definition of $f_{\alpha\beta}$, and the curvature free energy of the film is defined by

$$F_m = \int \frac{\kappa}{2}(H + c_0)^2 d\boldsymbol{a}, \tag{1.23}$$

where κ is the elastic constant of the film, c_0 is a spontaneous curvature governing the average geometry of the whole film surface and is originating from the molecular shape of the surfactant (for example, a corn-shaped molecules form a spherical film in the equilibrium state), and $d\boldsymbol{a}$ is the area element

of the membrane. Here the contribution from the surface tension is omitted for simplicity. Considering an almost planar film, we can define $\boldsymbol{R}$ as $\boldsymbol{R} = (x, y, h(x, y))$. In this case, the geometry of the film can be described on the cartesian coordinates $u = (x, y)$ instead of curvilinear coordinates. In this case, the mean curvature is given by

$$H \approx \frac{\partial^2 h}{\partial x^2} + \frac{\partial^2 h}{\partial y^2}, \tag{1.24}$$

and the curvature free energy of the almost planar film with $c_0 = 0$ is is given by

$$F_m = \int \frac{\kappa}{2} (\boldsymbol{\nabla}^2 h(x, y))^2 dxdy, \tag{1.25}$$

where the area element $d\boldsymbol{a}$ in the planar case is calculated as $d\boldsymbol{a} = \sqrt{d_g} dxdy \approx \sqrt{1 + |\boldsymbol{\nabla} h|^2} dxdy$ by using the approximation $d\boldsymbol{a} \approx dxdy$ with $h(x, y) \ll 1$. Then the statistical property of the membrane fluctuation is expressed in the Fourier space. $h(x, y)$ is Fourier transformed as follows,

$$h(x, y) = \frac{1}{N_\mathrm{s}} \sum_{\boldsymbol{q}} h_{\boldsymbol{q}} \exp(i\boldsymbol{q} \cdot \boldsymbol{x}), \tag{1.26}$$

where $h_{\boldsymbol{q}}$ is the amplitude of the Fourier mode of the fluctuation of the membrane that is composed of the surfactant molecules, $\boldsymbol{q} = (q_x, q_y)$ a wave vector in the Fourier space, $\boldsymbol{x} = (x, y)$ the coordinate on the cartesian space and N_s the total number of the surfactant molecules on the film (assuming a finite area of the film). Using Eq.1.26, Eq.1.25 can be written as follows,

$$F_m = \frac{A_\mathrm{m} \kappa}{2 N_\mathrm{s}^2} \sum_{\boldsymbol{q}} q^4 |h_{\boldsymbol{q}}|^2, \tag{1.27}$$

where $q = |\boldsymbol{q}|$ and A_m is the total area of the film. In this case, the probability density $P(h_{\boldsymbol{q}})$ is assumed to be proportional to $\exp(-\beta F_m)$ by the saddle point approximation, then the averaged value of the square of the amplitude $h_{\boldsymbol{q}}$ for a certain mode $\boldsymbol{q}$ is as follows,

$$\langle |h_{\boldsymbol{q}}|^2 \rangle = \frac{N_\mathrm{s}^2 k_\mathrm{B} T}{A_\mathrm{m} \kappa q^4}. \tag{1.28}$$

In this case, the dispersion of the amplitude $\langle |h_{\boldsymbol{q}}|^2 \rangle$ is very small for large wave number q according to Eq.(1.28). For a small q, the film tends to be

flat on the average but have large fluctuation since $\langle |h_{\boldsymbol{q}}|^2 \rangle$ is very large. Since the fluctuation with the small q follows Eq.1.28, we can estimate κ that is the physical property of the membrane by fitting Eq.1.28 to simulation data.

1.2.3 Membrane-confining system

In drug delivery system (DDS), which is one of the typical examples of membrane-confining system, a material (drug) is encapsulated into the membrane that is composed of surfactant or lipid, and transported to the target in human body. The capsule composed of surfactant or lipid molecules containing the drug is designed to dissociate at a certain region in our body as designed. The membrane may change the chemical properties through the chemical reaction for the composing materials in our body because the membrane confining the drug is affected by the environments and is deformed. Although the chemistry and the pharmacy of them are mainly important for the purpose of DDS, the physical properties of the membrane in our body are also important for various reasons. When the membrane exists in a narrow tube like blood vessels, its physical properties are important for the determination of its shape. Thus, the transformation of the membrane in DDS is coupled to the physical properties of its deformation. In addition, since the micellar structure is similar to our body cell, the properties are also similar. Although the drugs are usually polymers, some drugs are (low molecular weight) LC molecules on which we focus in the rest of this thesis.

As another application of LC contacting an interface, molecular sensor (MS) is an attractive example, which utilizes the anchoring through the interaction beetween LC molecule and a target molecule of MS. When the target approaches the LC close enough, the optical axis of LC phase rotates due to the anchoring and the change can be observed by the optical microscope. Then the existence of the target is easily detected. In many investigations of LC for MS, the researchers have focused on the configurations of the LC phase. So far only the case with rigid surface has been studied. However, when the surface can deform and fluctuate, more fascinating physics will emerge. We will address this problem in the following chapters.

1.2.4 Purpose of our study and outline of this thesis

When the interface fluctuates at the LC material interface, a non-trivial configuration of the LC orientation and/or the change in the shape of the

membrane at the interface can be observed due to the boundary conditions. LC orientation and the membrane shape are coupled since they interact with each other through the anchoring which governs the LC director relative to the membrane normal direction, resulting the configuration of such system including both LC and membrane complicated. Then, in chapter 2, we focus on the anchoring effect in the following chapters and estimate the physical properties of the membrane affected by the anchoring, which are of importance since they directly influence the formation of the membrane.

In chapter 4 , we will summarize about the effect of the anchoring and discuss some apprications.

Chapter 2

Method

2.1 Properties of interface on liquid crystal system

In the vicinity of a rigid boundary, the equilibrium configuration of the LC director is determined by competition between the LC elasticity and the anchoring working at the surface, resulting in determining the property of the fluctuation of the system only by them. On the other hand, in the case of a deforming boundary, the director, especially its fluctuation, affects the fluctuation of the surface. Since the anchoring gives the preferred orientation for the LC molecules at the interface, the deviation from the anchoring condition generates forces working on the LC director and the interfacial normal vector to eliminate the deviation, resulting in the fluctuational coupling. When an LC material contacts with an isotropic liquid or a gas phase, the director fluctuation of LC phase is coupled to the interfacial fluctuation at the interface [37]. In this case, the property of the fluctuation of the interface is modified by the director fluctuation through the anchoring interaction.

The behavior of LC at such an interface is remarkable in the case of a spherical droplet including LC phase contacting with an isotropic gas phase [38]. In this case, when the elasticity of the LC material is larger than the anchoring that induces the planar condition (Rull *et al.* realized this situation by using longer LC molecules), the LC droplet elongates due to the higher anisotropy of an interfacial tension. In other words, since the extrapolation length $b = K/W_a$ mentioned in Sec.1.1.2 increases (corresponding to weak anchoring), the contribution from the interfacial free energy to the LC

director becomes larger, leading to an elongation of the droplet [38].

In the case that a (fluctuational) membrane encloses the LC material, the properties of the interface including LC and membrane are also changed. According to Rey [39] who investigated analytically the interfacial properties of the membrane composed of the surfactant in contact with LC material, in the case of weak and homeotropic anchoring (the director prefers the interfacial normal at interface), the inverse of the interfacial fluctuation is dependent on $(\gamma_0 - W)q^2$, where W the anchoring strength and is negative value for homeotropic condition in [39], γ_0 the interfacial tenion of the membrane, and q is the absolute value of the wave vector parallel to the membrane tangential. Then the larger the anchoring strength is, the smaller the fluctuation of the interface becomes. On the other hand, when the strong anchoring case, the director field near the interface is governed by the interfacial normal ($\boldsymbol{n} = \boldsymbol{k}$ in [39], which $\boldsymbol{n}$ is the director and $\boldsymbol{k}$ is the interfacial normal), the gradient of the director field at the interface is changed by the interfacial fluctuation, resulting in Kq^3 behavior for the interfacial fluctuation, which K is the Frank elastic constant. These characteristic behaviors are attributed from the behavior confined into membrane.

LC phase at an interface that is either rigid or deformable shows a rich variety of physics including the formation of nematic layer and the fluctuational properties connected with the interfacial fluctuation. When the bulk LC phase is isotropic (then this phase is not "liquid crystal" phase), as was already mentioned, a nematic wetting layer may grow and is expected to compete with the fluctuation of the interface. To focus on these subtle behaviors, molecular simulation is a useful method since it can calculate the system with a microscopic molecular model but without a free energy. Since we are interested in the equilibrium properties of the phases, we conducted the simulation by Monte-Carlo method. In this section, we report some results on such system investigated by molecular simulation and analyze them by constructing a free energy model, mainly focusing on the interfacial properties covered by membrane interacting with LC through the anchoring.

2.2 Molecular simulation

2.2.1 Molecular models

For simplicity to estimate the interfacial physical properties affected by the confined LC material, we construct a lamella-like structure including single layer in a simulation system. The LC material is confined into a rectangular box, and the two monolayers composed of the surfactant molecules attach the LC material pointing to opposite direction each other as enclosing at top and bottom, so that it forms a wafer. The surfactant tail particles are just attached on the LC material surface. The membrane normal vector (Mnv) is defined as pointing to the direction from surfactant tail to its head particle, and defining the z-direction to the wafer surface normal, then the two Mnvs are parallel or anti-parallel to the z-direction. In this case, the single lamella is symmetric to $\boldsymbol{e}_z$. The region enclosed by the surface composed of the surfactant head particles is filled by a fluid of spherical, hydrophilic molecules. This system continues far away into x-y plane, so that the LC material is confined into two skins of monolayer of surfactants.

Since each molecules are modeled as coarse-grained molecules, they have some coarse-grained interaction potentials. The LC molecule is expressed by an ellipsoidal particle with only one symmetric axis as being parallel to the vector $\hat{\boldsymbol{u}}_i$. The corresponded potential is called Gay-Berne (GB) potential [40] as follows,

$$\begin{aligned} U_{\mathrm{GB}}(\boldsymbol{r}_{ij}, \hat{\boldsymbol{u}}_i, \hat{\boldsymbol{u}}_j) = 4\epsilon_{ij}[\epsilon_1(\hat{\boldsymbol{u}}_i, \hat{\boldsymbol{u}}_j)]^{\mu} \times [\epsilon_2(\hat{\boldsymbol{r}}_{ij}, \hat{\boldsymbol{u}}_i, \hat{\boldsymbol{u}}_j)]^{\nu} \\ \times \left([\varrho_{ij}(\boldsymbol{r}_{ij}, \hat{\boldsymbol{u}}_i, \hat{\boldsymbol{u}}_j)]^{-12} - [\varrho_{ij}(\boldsymbol{r}_{ij}, \hat{\boldsymbol{u}}_i, \hat{\boldsymbol{u}}_j)]^{-6} \right), \end{aligned} \tag{2.1}$$

where ϵ_{ij} is an interaction energy parameter of potentials between i and j particles, and $\boldsymbol{r}_{ij} = r_{ij}\hat{\boldsymbol{r}}_{ij}$ is a relative position vector, $r_{ij} = |\boldsymbol{r}_{ij}|$, and $\hat{\boldsymbol{r}}_{ij}$ is the relative direction vector. μ and ν are GB parameter. The three functions in 2.1 are described, $\epsilon_1(\hat{\boldsymbol{u}}_i, \hat{\boldsymbol{u}}_j)$, $\epsilon_2(\hat{\boldsymbol{r}}_{ij}, \hat{\boldsymbol{u}}_i, \hat{\boldsymbol{u}}_j)$, $\varrho_{ij}(\boldsymbol{r}_{ij}, \hat{\boldsymbol{u}}_i, \hat{\boldsymbol{u}}_j)$, as follows: first $\epsilon_1(\hat{\boldsymbol{u}}_i, \hat{\boldsymbol{u}}_j)$ is a measure of the magnitude of the energy and defined by

$$\epsilon_1(\hat{\boldsymbol{u}}_i, \hat{\boldsymbol{u}}_j) = [1 - \chi^2(\hat{\boldsymbol{u}}_i \cdot \hat{\boldsymbol{u}}_j)^2]^{-1/2}, \tag{2.2}$$

where $\chi = (\kappa^2 - 1)/(\kappa^2 + 1)$ and $\kappa{=}\sigma_{\mathrm{e}}/\sigma_0$, κ is an aspect ratio of the LC particle, where σ_0 is the size of LC particle of the short axis and σ_{e} being the size of symmetric long axis. The function $\epsilon_2(\hat{\boldsymbol{r}}_{ij}, \hat{\boldsymbol{u}}_i, \hat{\boldsymbol{u}}_j)$ is relative to the

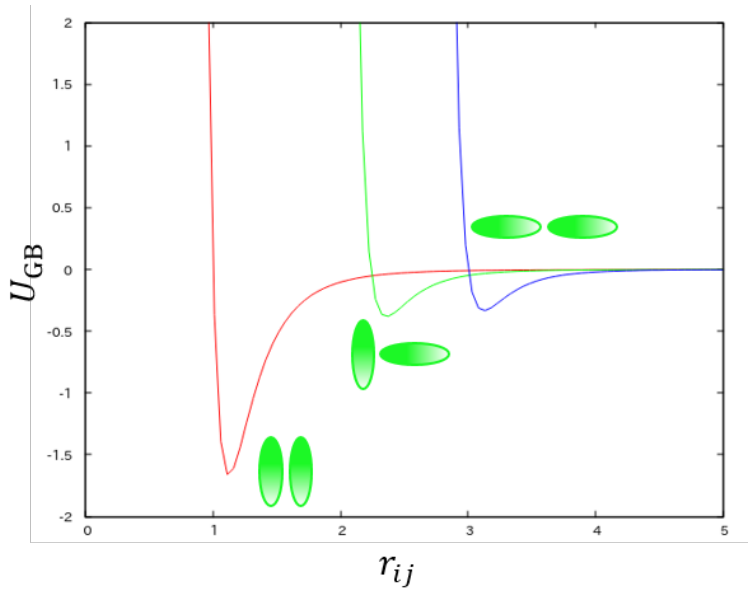

Fig. 2.1: The representative forms of the Gay-Berne potential $((\kappa, \kappa', \mu, \nu)=(3.0, 5.0, 2.0, 1.0)$ are the same parameter set as used in our simulation). The combinations of the ellipsoids in this picture are the corresponding configuration for the respective form of potential. The ratio of the energy depth of the side-by-side configuration (corresponding to the deepest energy depth, red line) to that of the end-to-end configuration (corresponding to the shallowest energy depth, blue line) shows the value of $\kappa' = 5.0$.

angle between the long axes $\hat{\boldsymbol{u}}_i$ and the relative direction vector $\hat{\boldsymbol{r}}_{ij}$ of two ellipsoidal particles and defined by following expression,

$$\epsilon_2(\hat{\boldsymbol{r}}_{ij}, \hat{\boldsymbol{u}}_i, \hat{\boldsymbol{u}}_j) = 1 - \chi' \left[\frac{(\hat{\boldsymbol{r}}_{ij} \cdot \hat{\boldsymbol{u}}_i)^2 + (\hat{\boldsymbol{r}}_{ij} \cdot \hat{\boldsymbol{u}}_j)^2 - 2\chi'(\hat{\boldsymbol{r}}_{ij} \cdot \hat{\boldsymbol{u}}_i)(\hat{\boldsymbol{r}}_{ij} \cdot \hat{\boldsymbol{u}}_j)(\hat{\boldsymbol{u}}_i \cdot \hat{\boldsymbol{u}}_j)}{1 - \chi'^2(\hat{\boldsymbol{u}}_i \cdot \hat{\boldsymbol{u}}_j)^2} \right], \tag{2.3}$$

where $\chi'=(\kappa'^{1/\mu} - 1)/(\kappa'^{1/\mu} + 1)$ and $\kappa'=\epsilon_{\rm ee}/\epsilon_{\rm ss}$, κ' is the interaction energy depth ratio between end-to-end ($\epsilon_{\rm ee}$), which shows that the long axes are just on a common line, and side-by-side ($\epsilon_{\rm ss}$), which that the short axes being on the common line, configurations of two ellipsoidal particles (see Fig.2.1).

Finally, $\varrho_{ij}(\boldsymbol{r}_{ij}, \hat{\boldsymbol{u}}_i, \hat{\boldsymbol{u}}_j)$ is defined by

$$\varrho_{ij}(\boldsymbol{r}_{ij}, \hat{\boldsymbol{u}}_i, \hat{\boldsymbol{u}}_j) = \frac{r_{ij} - \sigma(\hat{\boldsymbol{r}}_{ij}, \hat{\boldsymbol{u}}_i, \hat{\boldsymbol{u}}_j) + \sigma_{ij}}{\sigma_{ij}}, \tag{2.4}$$

where $\sigma(\hat{\boldsymbol{r}}_{ij}, \hat{\boldsymbol{u}}_i, \hat{\boldsymbol{u}}_j)$ is defined as

$$\sigma(\hat{\boldsymbol{r}}_{ij}, \hat{\boldsymbol{u}}_i, \hat{\boldsymbol{u}}_j) = \sigma_{ij} \left(1 - \chi \left[\frac{(\hat{\boldsymbol{r}}_{ij} \cdot \hat{\boldsymbol{u}}_i)^2 + (\hat{\boldsymbol{r}}_{ij} \cdot \hat{\boldsymbol{u}}_j)^2 - 2\chi(\hat{\boldsymbol{r}}_{ij} \cdot \hat{\boldsymbol{u}}_i)(\hat{\boldsymbol{r}}_{ij} \cdot \hat{\boldsymbol{u}}_j)(\hat{\boldsymbol{u}}_i \cdot \hat{\boldsymbol{u}}_j)}{1 - \chi^2(\hat{\boldsymbol{u}}_i \cdot \hat{\boldsymbol{u}}_j)^2} \right] \right)^{-1/2}. \tag{2.5}$$

σ_{ij} is the size parameter of potentials between i and j particles. The four GB parameters (κ, κ', μ, ν) of U_{GB} for representing the ellipsoidal LC particle, σ_0, and ϵ_0, as being the size unit and energy unit in potentials, are given later.

The surfactant molecule is composed of three spherical beads, which includes two types for the hydrophilicity, one is the hydrophilic "head" particle and another the hydrophobic "tail" particle, explained in Sec.1.2.1. One particle of three beads is the head particle, and others are the tail particles. These particles have Lennard-Jones (LJ) potential described by

$$U_{\mathrm{LJ}}(r_{ij}) = 4\epsilon_{ij} \left(\left(\frac{\sigma_{ij}}{r_{ij}} \right)^{12} - \left(\frac{\sigma_{ij}}{r_{ij}} \right)^{6} \right). \tag{2.6}$$

This is the spherical symmetric potential in distance space and can express the spherical particle, especially expressing the properties of rare gas atoms. In molecular simulation, since such potential is frequently used to describe liquids and is almost succesful, we use it not only for spherical particles of surfactant but also for spherical one constructing hydrophilic fluid filled in the region between the head particle sheets.

The consecutive particles in one surfactant molecule are connected by the following spring potential,

$$U_{\mathrm{spring}}(r_{ij}) = \frac{1}{2} k_{\mathrm{spring}} (r_{ij} - \sigma_{ij})^2, \tag{2.7}$$

where k_{spring} is the energy constant of the spring. The surfactant molecule with short length is generally rigid, which is expressed by the following bending potential,

$$U_{\mathrm{bend}}(\theta) = k_{\mathrm{bend}}(1 - \cos(\theta - \theta_0)), \tag{2.8}$$

where $k_{\rm bend}$ is the bending energy constant, θ corresponds to the angle composed of the two consecutive bonds of the surfactant molecule, and θ_0 means an equilibrium angle of these bonds, we put $\theta_0 = 0$ in this thesis, so that our model of the surfactant is often lineary.

Here, we introduce an important potential between ellipsoidal (labeled i) and sphirical (labeled j) particles (labeled "sg" which represents "spherical particle and GB particle" as subscript) as follows:

$$U_{\rm sg}(\boldsymbol{r}_{ij},\hat{\boldsymbol{u}}_i) = 4\epsilon_{ij}[\epsilon_{\rm sg}(\hat{\boldsymbol{r}}_{ij},\hat{\boldsymbol{u}}_i)]^{\mu} \times \left([\varrho_{{\rm sg}ij}(\boldsymbol{r}_{ij},\hat{\boldsymbol{u}}_i)]^{-12} - [\varrho_{{\rm sg}ij}(\boldsymbol{r}_{ij},\hat{\boldsymbol{u}}_i)]^{-6}\right), \tag{2.9}$$

$$\varrho_{{\rm sg}ij}(\boldsymbol{r}_{ij},\hat{\boldsymbol{u}}_i) = \frac{r_{ij} - \sigma_{\rm sg}(\hat{\boldsymbol{r}}_{ij},\hat{\boldsymbol{u}}_i) + \sigma_{ij}}{\sigma_{ij}}, \tag{2.10}$$

$$\sigma_{\rm sg}(\hat{\boldsymbol{r}}_{ij},\hat{\boldsymbol{u}}_i) = \sigma_{ij}\left[1 - \chi(\hat{\boldsymbol{r}}_{ij}\cdot\hat{\boldsymbol{u}}_i)^2\right]^{-1/2}, \tag{2.11}$$

$$\epsilon_{\rm sg}(\hat{\boldsymbol{r}}_{ij},\hat{\boldsymbol{u}}_i) = 1 - \chi'_{\rm sg}(\hat{\boldsymbol{r}}_{ij}\cdot\hat{\boldsymbol{u}}_i)^2, \tag{2.12}$$

where $\chi'_{\rm sg} = 1 - \xi^{1/\mu}$ and $\xi = \epsilon_{\rm E}/\epsilon_{\rm S}$. $\epsilon_{\rm E}$ in ξ ("E" means "End" point of ellipsoid) is the energy depth in the case that the long axis vector of the ellipsoidal particle is directed to the spherical one, and $\epsilon_{\rm S}$ ("S" means "Side" of ellipsoid) is the energy depth in the case that the short axis of ellipsoidal particle is directed to the spherical one. The shape of the potential function is shown in Fig.2.2.

ξ will be called the anchoring parameter throughout this thesis and characterizes the anisotropic interaction as being able to understand from the fact that it is the parameter of the coefficient of $(\hat{\boldsymbol{r}}_{ij}\cdot\hat{\boldsymbol{u}}_i)^2$. Then the anisotropic interaction potential $U_{\rm sg}$ includes the effect of the anchoring, whose value changes depending on the direction of the ellipsidal particle to the interacting spherical one and is measured by the parameter ξ. In realistic system, anchoring effects are realized by some interactions and now we limited it in the anisotropic Van der Waals interaction, which is given by the surface-covered molecules or the surface-penetrated one approacing from outer region. Although it should be written by a function of the concentration of these interacted molecules, we attempt to systematically change ξ to investigate its influence to our model system. In our work this anchoring parameter ξ plays an important role.

The interactions between particles of the different types are either attractive or repulsive, which the repulsive interaction is expressed by using only the positive term in all non-bonded interaction potentials (corresponds to a

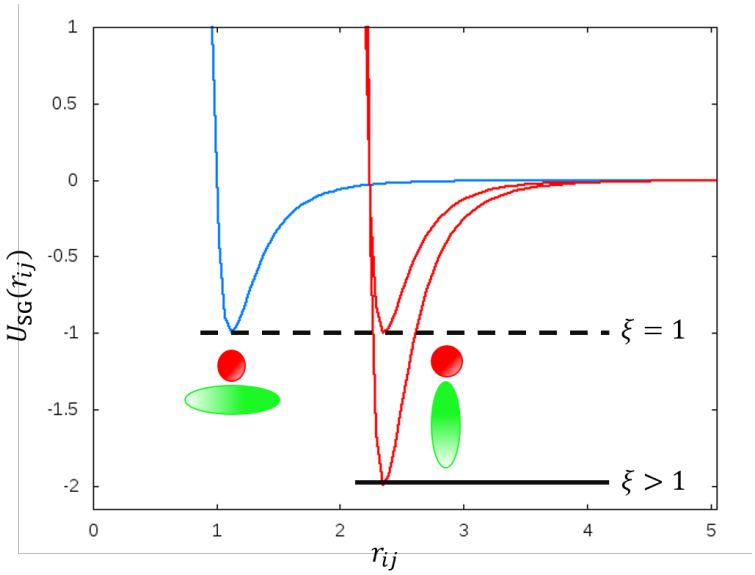

Fig. 2.2: The representative potential functions of $U_{\rm sg}$ are shown: one corresponds to the configuration that the LC long axis orients to the spherical particle, and another corresponds to that the LC short axis orients to the spherical particle. The potentials that contact the dot line at its deepst point have the value of the parameter $\xi = 1.0$, whereas the potential that contact the solid line has $\xi > 1.0$.

soft-core potential) in our work. The LC particles are attractive to the tail particles of surfactants, while it is repulsive to the heads of surfactants and hydrophilic ones, the tails are repulsive to the heads and hydrophilic ones, and the heads are attractive to hydrophilic ones. Due to these combinations of the interactions, the interfacial tension between LC and hydrophilic particles is larger than the attractive case, and the surface activity of the surfactants is emphasized, so that the lamella structure of our model is stable in terms of the interaction. Such combinations of interactions also give the concentration of the effect of the anchoring between the LC and the tail particle, because the anchoring effect is realized mainly by the attractive term of Eq.(2.9) (repulsive term is also changed by changing anchoring, but that is tiny). Then, the observed behaviors of these phases of LC and surfactant membrane are caused mainly from the interaction between them.

2.2.2 Parameters of potentials

Here, we give the values of the parameters used in our simulations. The interaction energy parameter ϵ_{ij} for all combinations of particles are the same value according to the combinations of interacting particles, ϵ_{00}=ϵ_{11}=ϵ_{22}=ϵ_{33}=ϵ_0, where the subscript i=0,1,2 and 3 mean surfactant head, surfactant tail, hydrophilic particle, and LC particle, respectively. ϵ_0 is the energy unit in our simulation and is equal to $k_{\rm B}T_{\rm r}$, where $k_{\rm B}$ is the Boltzmann constant, and $T_{\rm r} = 300[K]$ is a room temperature. Using this energy unit, the dimensionless temperature is defined by T^*=$k_{\rm B}T/\epsilon_0 = T/T_{\rm r}$ as the ratio of the temperature to the room one in our simulation. $\epsilon_{i,j}$=$\sqrt{\epsilon_{ii}\epsilon_{jj}}$ simply. The diameter of the spherical particles and the minor axis length of the ellipsoid is as following: σ_{00}=1.05σ_0, σ_{11}=1.0σ_0, σ_{22}=1.0σ_0, σ_{33}=1.0σ_0, and σ_0 is the unit of length, and $\sigma_{i,j}$=$(\sigma_{ii} + \sigma_{jj})/2$, simply. The sizes of the surfactant head and tail are determined from Lipowsky [41], where surfactant models are more detailed than ours, but we more coarse-graining. Actual surfactants almost have a large head and relatively slender tail, so that set of diameters is natural. Other particle sizes are determined simply to be the same as the size of the surfactant tail. The spring energy $k_{\rm spring}$ of the surfactant molecule is $100\epsilon_0/\sigma_0^2$ and the bending energy $k_{\rm bend}$ is $10\epsilon_0$ referred to [41], and coarse-grained above mentioned. The four GB parameters determining the form of ellipsoids are chosen as $(\kappa, \kappa', \mu, \nu)$=$(3.0, 5.0, 2.0, 1.0)$ which are originally used by Gay and Berne in [40]. These molecular models are very simple models to interpret the change in the anchoring parameter due to the same energy parameters. Since our purpose is to estimate the membrane physical properties which are affected by the confined LC, we prevented from setting the actual molecules.

2.2.3 How to propagate system based on Monte-Carlo method

As mentioned above, we conducted the molecular simulation with Monte-Carlo method. In Monte-Carlo simulation, a new configuration is changed to the lower energy state basically, but the slightly higher energy states are probably adopted. The transition probability between configurations is obtained by constant temperature and pressure ensamble (of course the number

of particles is constant),

$$P_{\rm tr}(j \to i) = \min\left(1, \exp\left(-\beta\delta U_{{\rm tot},ij} - P(V_i - V_j) - N\log\frac{V_j}{V_i}\right)\right). \qquad (2.13)$$

The subscripts i and j indicate the configurations, where i is the new configuration (candidate) and j is the current configuration. $\delta U_{{\rm tot},ij} = U_{{\rm tot},i} - U_{{\rm tot},j}$ is the difference of the total energy between i and j configurations, and $V_i - V_j$ is the volume difference. Parameters N, P and $\beta = 1/(k_{\rm B}T)$ determine the equilibrium state. The dimensionless pressure is defined as $P^* = P\sigma_0^3/\epsilon_0 = 3.0$ in our simulation. For this pressure and the dimensionless temperature $T^* \approx 1.0$, our LC material is in the isotropic phase near the nematic region (phase diagram is given in [42]). The total number of the particles N=115,200 that is composed of the number of the surfactants $N_{\rm s}$=6,400, the LCs $N_{\rm l}$=51,200, and the hydrophilic particles $N_{\rm w}$=44,800, respectively.

To estimate the physical properties in the equilibrium state, first we prepare an LC-surfactant monolayer lamella floating in a hydrophilic fluid as an initial state of the simulation system, and take $1 \sim 2\times10^5$ MCS to obtain the minimum energy state. In the case with lower temperature or with higher κ' in GB potential which gives the higher elastic properties, a larger number of MCS is necessary for the equilibrium. After such an equilibration process, we again perform 1.0×10^5 MCS to obtain 500 snapshots. Such calculation is independently conducted 3$\sim$5 times to obtain the averaged physical properties (we conducted these "independent" simulations starting from different initial states).

Chapter 3

Result

3.1 Results of molecular simulation

In this section, first we show the physical properties of the membrane estimated by molecular simulation mentioned in the previous chapter. Second, we compare the above results with another type of systems, i.e. the oil-confined systems where the oil is composed of spherical particles. In the simulation of the oil-confined system, the LC particles are replaced by the spherical oil particles which interact with the same interaction potential as the free-tail-particle of the surfactant (non-bonded one). Thus, the oil particle interacts attractively with the surfactant tail particles, and repulsively with the head and the hydrophilic particles. The size of the oil particle is the same as that of the tail particle σ_0, which has a smaller volume than that of the LC particle. The difference in the particle volume and in the molecular shape can affect the physical properties of the membrane.

Figures 3.1 and 3.2 are the "effective" interfacial tension γ_{eff} and the "effective" bending rigidity K_{eff} of the membrane in the LC-confined system, where both quantities are dimensionless values. The "effective" means that these values are estimated directly from the results of simulations including the influence from the LC material by using the following equations;

$$\langle |h_{\boldsymbol{q}}|^2 \rangle = \frac{N_{\text{s}}^2 k_{\text{B}} T}{A_{\text{m}} K_{\text{eff}} q^4}, q < 1, \tag{3.1}$$

$$\langle |h_{\boldsymbol{q}}|^2 \rangle = \frac{N_{\text{s}}^2 k_{\text{B}} T}{A_{\text{m}} \gamma_{\text{eff}} q^2}, q > 1, \tag{3.2}$$

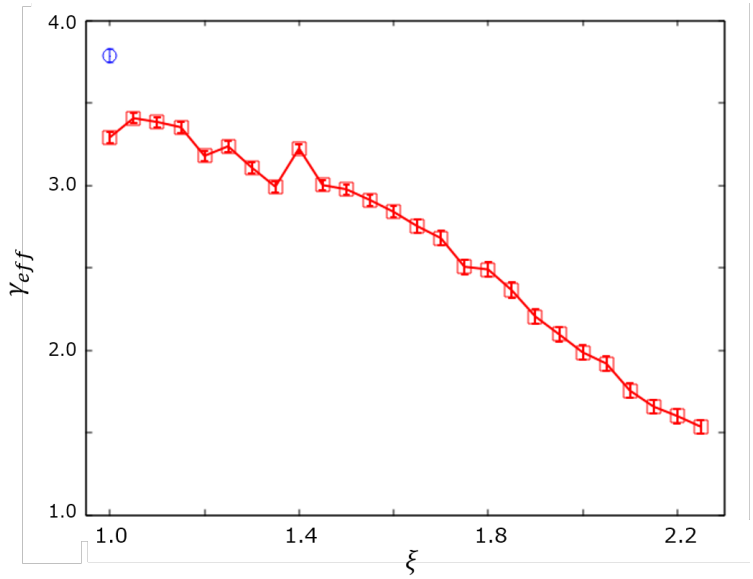

Fig. 3.1: The red line shows the dimensionless interfacial tension of the membrane γ_{eff} as a function of the anchoring parameter ξ. The blue data at $\xi = 1$ shows the interfacial tension γ_0 for the case with the spherical oil confined system (the interaction energy between oil and surfactant tails is $\epsilon_0 = 1$).

which are calculated analytically by the same approach of Eq.1.28 but with the effective interfacial tension γ_{eff} in the free energy Eq.1.23. These expressions are not limited to the surfactant membranes but also applicable to the interfaces of the system constructed by the membrane and the LC material (and of course the hydrophilic fluid). The quantities γ_{eff} and K_{eff} are functions of the anchoring parameter ξ which is defined in Sec.2.2.1. For example, in Fig.3.1, γ_{eff} changes as a quadratic function of ξ. Since the (anisotropic) attractive interaction energy between an LC particle and a tail particle of the surfactant is increased by increasing ξ according to Eq.2.9, it can be intuitively understood that γ_{eff} decreases when ξ increases (When the Gibbs enthalpy difference is denoted as $\Delta G = A_{\text{m}}\Delta\gamma$, where A_{m} is the area of the membrane and $\Delta\gamma$ is the interfacial tension difference, the increase in the interaction energy makes ΔG decreased and accordingly γ_{eff} is decreased). In this case, the area of the system in the planar direction along the membrane

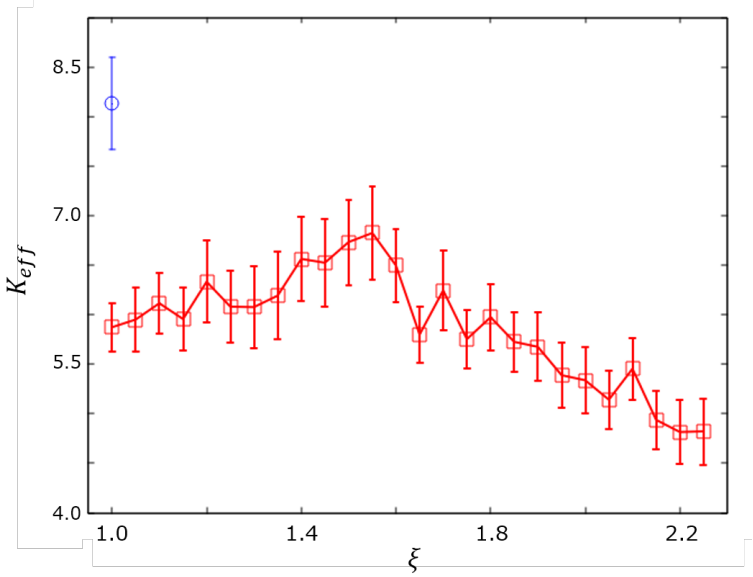

Fig. 3.2: The red line shows the dimensionless bending rigidity of the membrane $K_{\rm eff}$ as a function of the anchoring parameter ξ. The blue data at $\xi = 1$ shows the bending rigidity K_0 in the spherical oil confined system (the interaction energy between spherical oil and surfactant tails is $\epsilon_0 = 1$).

is increased due to the constant pressure condition when the increase in the attractive interaction energy between the tail particles and the LC particles contacting at the interface, resulting in the decrease in the distance between two membranes due to an imcompressibility condition of the LC material. If the distance is very small, two membranes may interact with each other, which will affect the membrane properties. However, the minimum distance between them in our work for LC-confined system is thick enough to estimate their properties independently. The dimensionless area $A^*_{\rm m} = A_{\rm m}/\sigma_0^2$ and the dimensionless thickness $l^*_m = l_m/\sigma_0$ are plotted as functions of ξ in Fig.3.3 ((a) for $A^*_{\rm m}$, (b) for l^*_m, respectively), where * is omitted for simplicity. The minimum thickness is about $40\sigma_0$, which corresponds to about 13 molecular layers composed of the LC particles oriented in the layer normal direction. In our simulation, since no layer exists in the LC phase (because it is in the isotropic or weak nematic phase), we can exclude the effect of the interaction between the fluctuations of two or more layers of LC material through the

bluk.

Here, we define the corrected interfacial tension including the pressure effect as $\gamma_{\mathrm{eff,P}} = \gamma_{\mathrm{eff}} - P$, where $P = 3.0$ is set as the dimensionless pressure in our simulation as mentioned in Sec.2.2.3. Since γ_{eff} takes the value $\gamma_{\mathrm{eff}} = 3.0$ arround $\xi = 1.4 \sim 1.5$ which gives $\gamma_{\mathrm{eff,P}} = 0$, the equilibrium membrane area may be achieved around $\xi = 1.4 \sim 1.5$. For the equilibrium area, the surfactant density has its equilibrium value. If in this case, since the density goes through the equilibrium at $\xi \sim 1.5$, the tendency of K_{eff} may change at the point on ξ axis. If the interaction energy parameter kept constant, increasing the area from lower side of the equilibrium value of the membrane to larger side by an external force, the interfacial tension changes from the negative to the positive value across the equilibrium value $\gamma_{\mathrm{eff,P}} = 0$ [43] (for pressure-free condition). In addition, the bending rigidity is lower for compressed membrane than that for expanded one because the compressed membrane tends to fluctuate largely to derive larger area. In this case, K increases by expanding the membrane area around the equilibrium area. The increase in the bending rigidity by increasing area is as follows : if the membrane is expanded over the equilibrium area by an external force, the surfactant molecules on the expanded membrane tend to decrease their distance, then the membrane less fluctuates to prevent from deriving the excess area. In our simulation, since the depth of the (attractive) interaction energy is changed due to the change in ξ, it is difficult to understand the behaviors of γ_{eff} and K_{eff} from the change in the equilibrium area ((a) in Fig.3.3) and the effect of the pressure.

Figure 3.4 shows the two types of the LC (scalar) order parameters, where the red line corresponds to the maximum value of the order parameter $S_{\max}$ near the interfacial region of the LC phase, and the blue one to the order parameter value at "just" interface between LC and membrane S_{int} (S_{int} is estimated at the point where the number density of the LC particle shows the half value of that at the bulk region. At this region, since, averagely, the LC particles contact the surfactant molecules, the word "just" is used.). To evaluate these scalar order parameters, we calculated the tensor order parameter $\boldsymbol{Q}(\boldsymbol{r})$ by

$$\boldsymbol{Q}(\boldsymbol{r}) = \langle \boldsymbol{u}\boldsymbol{u} - \frac{\mathbf{1}}{3} \rangle, \tag{3.3}$$

where $\boldsymbol{u}(\boldsymbol{r})$ is a molecular axis vectors and $\langle \cdot \rangle$ means the average for LC particles in a small cell at $\boldsymbol{r}$. This tensor $\boldsymbol{Q}(\boldsymbol{r})$ is then orthogonalized to obtain 3 eigenvalues. The maximum value among this 3 eigenvalues is the

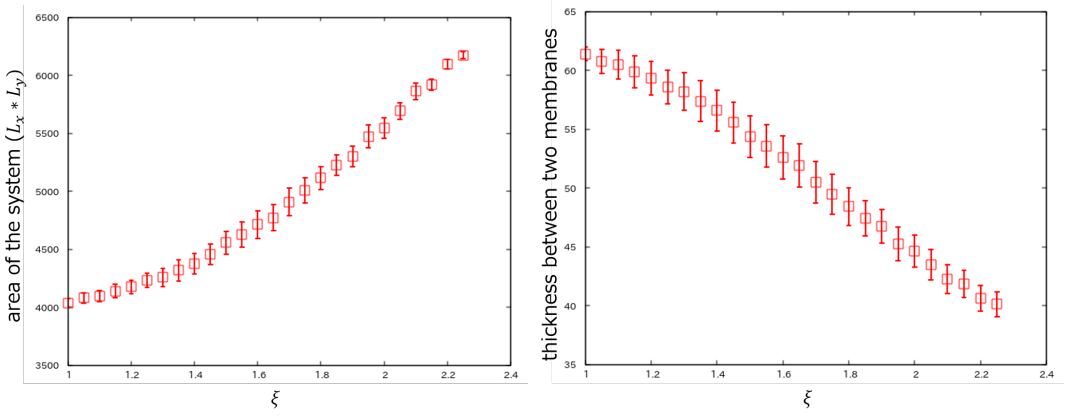

(a) **(b)**

Fig. 3.3: (a) The dimensionless area of the system, and (b) the dimensionless thickness between two membranes for the anchoring parameter ξ.

scalar order parameter $S(\boldsymbol{r})$ of the weak nematic phase with the eigenvector (director) $\boldsymbol{n}(\boldsymbol{r})$ (when in the uniaxial nematic phase, one can construct $\boldsymbol{Q}(\boldsymbol{r})$ using $S(\boldsymbol{r})$ and $\boldsymbol{n}(\boldsymbol{r})$ as defined in Sec.1.1.1). The cell size used to average molecular axis vectors is determined by $(a_x, a_y, a_z) = (L_x/b_x, L_y/b_y, L_z/b_z)$, where L_α is the size of the system in α-direction ($\alpha = x, y, z$) and b_α is the number of the cells when accounts them for α-direction. The coordinate system is cartesian system as mentioned in the beginning of Sec.2.2.1, where z-direction is in the average direction of the membrane normal and the plane along the membrane corresponds to $x - y$ plane. An LC particle is allocated into a cell at $\boldsymbol{r}$ to estimate $\boldsymbol{Q}(\boldsymbol{r})$ but a problem may occur in the calculation of $\boldsymbol{Q}(\boldsymbol{r})$ due to the variable size of the defined cell. The size of the cell in each direction can change due to the constant pressure condition resulting in the anisotropic shape of the cell. By the change in the cell shape, the spatial distribution of the tensor order parameter field $\boldsymbol{Q}(\boldsymbol{r})$ calculated in the cells may be changed without the change in the LC molecular orientation. To prevent above calculation error, we took two counterplans as follows: i) the average cell size was taken not to be over the LC molecular size ($3\sigma_0$ about the long axis length of the ellipsoids since the aspect ratio is $\kappa = 3.0$ as mentioned in Sec.2.2.2); ii) the LC particles were divided in the long axis length, $3\sigma_0$, by σ_0. Information of the molecular orientation of the LC particle was allocated into its divided components in the long axis. By the

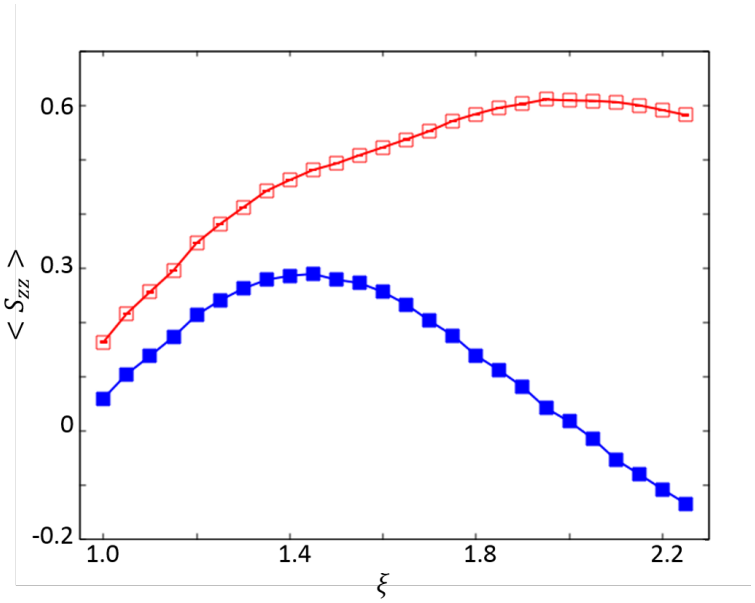

Fig. 3.4: The red (blue) line shows the change in the LC scalar order parameter with maximum value in the LC material $S_{\max}$ (order parameter at the interfacial position S_{int}) with anchoring ξ.

operation, the anisotropy of the cell size is expected to be little problem for the estimation of $\boldsymbol{Q}(\boldsymbol{r})$. Consequently, we can draw the profile of $S(\boldsymbol{r})$ at each area element at $(x_i, y_j) = (i * a_x, j * a_y)$ with the size (a_x, a_y) in z-direction to the interface point $\boldsymbol{r}_{\text{int}}$, where the number density becomes the half of that at the center region. Since our system has two membranes, we calculate the $S(x_i, y_j, z)$ profile in the z-direction from the interface at one membrane to that at another membrane. Then, by averaging $S(x_i, y_j, z)$ in the $x - y$ plane at a position z, we can get the z profile of the LC order parameter $S(z)$ as in Fig.3.5. In Fig.3.5, $S(z)$ shows higher value near the interface (near the both side of these graphs) than that in the center region. This means that a quasi-nematic wetting layer (but it disappears quickly as going away from the interface) grows although some decreasing behaviors of $S(z)$ are also appeared at both sides in Fig.3.5.

In the $S(x_i, y_j, z)$ profile in the z-direction, we can confirm its maximum value near the interface (Its profile is almost similar to the averaged $S(z)$ profile in Fig.3.5). Then we get the profile of the maximum $S(x_i, y_j, z)$ in the

planar direction along the membrane and average in the planar direction, resulting in obtaining $S_{\max}$ (Of course we calculate independently $S_{\max}$ at each membrane, and average two values of $S_{\max}$). In addition, we get $S(x_i, y_j, z)$ at $\boldsymbol{r}_{\text{int}}$ and average in the planar direction as well as $S_{\max}$.

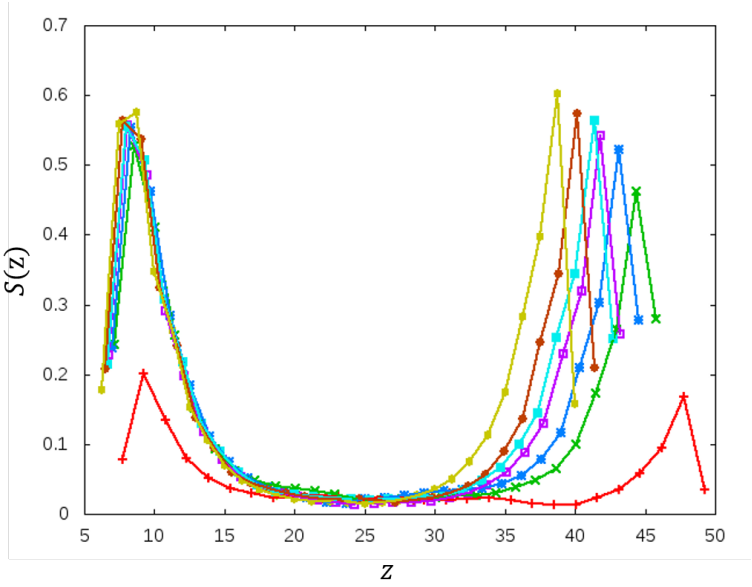

Fig. 3.5: These are the scalar order parameter profile in z-direction: red line is $\xi = 1.0$, green $\xi = 1.45$, blue $\xi = 1.5$, purple $\xi = 1.65$, sky blue $\xi = 1.7$, brown $\xi = 1.75$ and yellow $\xi = 1.8$, respectively.

According to Fig.3.4, $S_{\max}$ almost increases for an increase in ξ and approaches a threshold value. On the other hand S_{int} also increases up to $\xi \sim 1.4$, where it starts to decrease to a negative value. Note that $S = 0$ means the isotropy for the LC orientaion but the negative S means that the LC particles orient into the $x - y$ direction (membrane surface direction), can be seen in Fig.3.6. In these figures, the LC material near the membrane is shown, but the membrane is not, which is actually on the upper side of the LC material in each figures. From these figures, it is observed that on the upper side, the number of the LC particles orienting into the surface direction increases by increasing ξ. If only the anchoring effect characterized by ξ worked, the LC orientation near the membrane would be parallel to the membrane normal by increasing ξ due to the strong anisotropy of the attrac-

tive interaction between the LC and the tail particles (see Eq.2.9. Actually $S_{\max}$ shows that effect.). In such a region, S_{int} shows a different behavior. One of the reasons of this behavior will be the increase in the attractive interaction between LC and tail particle at the edge of the LC ellipsoidal particle. Then, the horizontal orientation of the LC particle to the membrane results in a stronger interaction than the normal orientation case because the number of the interaction points increased. However, as long as concerning γ_{eff} (Fig.3.1) and the surface area ((a) in Fig.3.3), both values do not show the drastic change near $\xi \sim 1.4$. Thus, the increase in the number of horizontally oriented LC particles gives little effect on the interfacial properties. Therefore, we can expect that the change in S_{int} originates from the change in the other properties, for example the bending regidity K_{eff}.

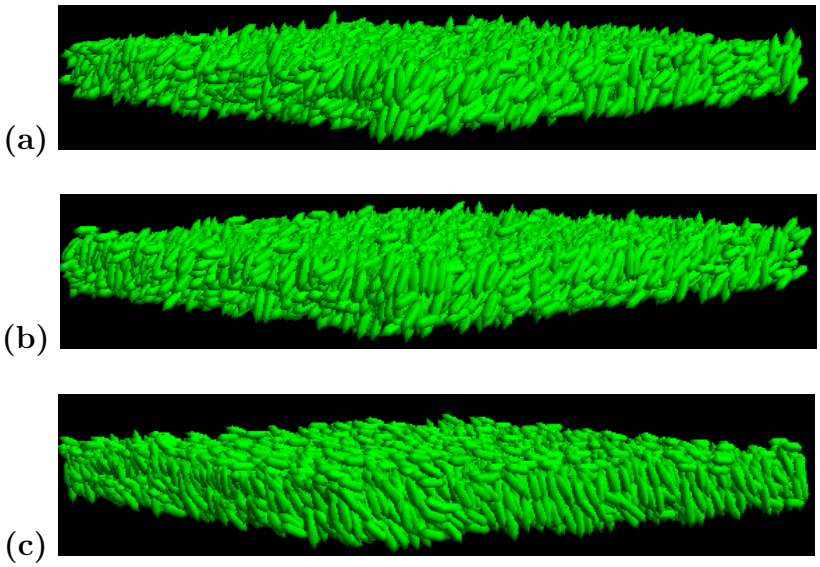

Fig. 3.6: Snapshot of the LC material near the interface. (a) $\xi = 1.0$, (b) $\xi = 1.4$, (c) $\xi = 1.8$.

Other reasons for the changes in γ_{eff} and K_{eff} may be related to the penetration of the LC particles into the membrane since the LC particle interacts attractively with the tail particle of the surfactant molecule and interacts stronger by increasing ξ (Note that the interaction between them is anisotropic according to Fig.2.2. The depth of the potential with the configuration that the short axis of the LC particle orients to the spherical

one is smaller than that with the configuration that the long axis of the LC particle orients to the spherical one, in the case with $\xi > 1$.). In general case that the surfactant membrane confines a fluid, the penetration of the particles constructing the fluid may soften the membrane: in equilibrium state, as the particles come in or out from the membrane, the membrane may become easier to expand or shrink around its equilibrium area (that is, its area fluctuation may become larger by the penetration). The smaller the size of the penetrating particle is, the stronger the penetration effect becomes. In our case, however, the LC particles have the size similar to the size of the surfactant molecules. Since the large volume is necessary for the LC particles to penetrate into membrane, the density of the LC particles penetrating into the membrane is small.

In addition, since the attractive interaction between the LC particle and the tail particle of the surfactant molecule becomes stronger by increasing ξ, the penetrating LC particles constrain the surfactant molecules to be around theirself in order to realize the potential energy minimum. In this case, since the area fluctuation of the membrane becomes smaller, the interfacial tension increases. However, in our case, γ_{eff} decreases by increasing ξ (see Fig.3.1).

More unexpected behavior for the penetration effect is observed in the behavior of K_{eff}. If the density of the penetrating LC particles into the membrane became larger by increasing ξ, the contribution of the LC elasticity for the membrane would become larger. The larger LC elasticity is, the larger the bending rigidity of the membrane becomes. However, K_{eff} shows the non-monotonic behavior: it would be expected that the bending rigidity shows the monotonic increasing behavior as a function of ξ if the penetration density became larger.

Thus, the penetration effect of the LC particles for the membrane is very small although a few LC particles penetrate. Figure 3.7 shows the distribution of the LC particles per the cell volume (defined as the same as for the estimation of $S(\boldsymbol{r})$), which is the function of the distance from the surfactant head position. The head position is $z = 0$, and on the average the last tail particle is located at $z \approx 2.0$. According to Fig.3.7, it can be observed that the number of the LC particles at $z \approx 2.0$ increases by increasing ξ (see (a) in Fig.3.7), so that actually a slight LC particles may penetrate into the membrane. In addition, the penetrating LC molecules tend to orient along the membrane by increasing ξ due to the more attractive interaction in the case that the LC long axis orients to the tail particle of the surfactant molecule. In this case, the more the number of the penetrating LC particles

is, the smaller the LC order parameter at the interface. Actually $S_{\rm int}$ shows the decreasing behavior at $\xi > 1.4$. However, from above discussion, the penetration does not much occur, then the behavior of $S_{\rm int}$ is influenced by other effect. Of course the reason of the changes in $\gamma_{\rm eff}$ and $K_{\rm eff}$ may be different from the penetration, it will be discussed later.

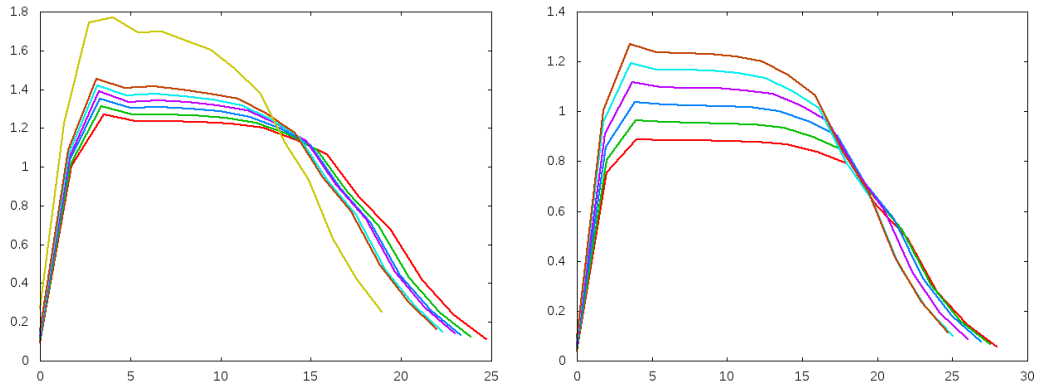

(a) **(b)**

Fig. 3.7: The distributions of the LC particles estimated for the distance from the surfactant head position (the head position is $z = 0$).

To compare above discussion for the fluid, which is composed of large and anisotropic particles, confined system, we also performed a different simulation confining a simple fluid composed of spherical particles that is oily molecules: the element particle of the simple oily fluid, which we call hereafter "oil particle" or simply "oil", interacts attractively with itself and the tail particle of the surfactant molecule (via Eq.2.6), whereas interacts repulsively with the head particle of the surfactant molecule and the hydrophilic particle being outside the membrane (via the repulsive part of Eq.2.6). The size of the oil particle is equal to σ_{33} that is the size of the short axis of the LC particle. Only the interaction energy parameter between the tail and the oil particle $\epsilon_{1,3}$ ("1" shows the tail particle, "3" the oil one) is changed in this simulation for $\epsilon_{1,3} = 1.0\epsilon_0 \sim 1.75\epsilon_0$, however other energy parameters, $\epsilon_{0,3}$, $\epsilon_{2,3}$ and ϵ_{33} are the same value as the case of the LC particle, that is, $\epsilon_{i,3} = 1.0, i = 0, 2, 3$. Using above defined particle, we estimated the interfacial tension and the bending rigidity of the interface as similar to the LC-confined case.

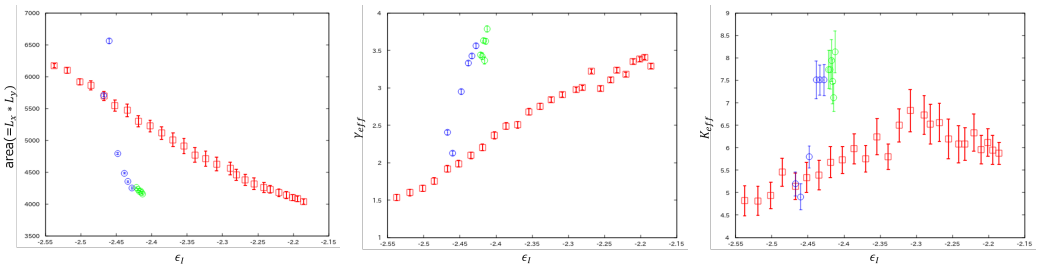

(a) **(b)** **(c)**

Fig. 3.8: The comparison of the area (a), the interfacial tension (b) and the bending rigidity (c) of the interface between the LC and the oil-confined system for the interfacial potential energy per one particle. On the transverse axis, the positive direction is taken in the right direction.

The results are shown in Fig.3.8 for the area (a), the interfacial tension (b) and the bending regidity (c) of the interface as functions of the interaction energy near the interface per one particle (Defined as $\epsilon_{\rm I} = E_{\rm tot}^{\rm int}/N^{\rm int}$, where $E_{\rm tot}^{\rm int}$ is the total interaction energy near the interface and $N^{\rm int}$ is the total number of the particle near the interface which includes the oil (or LC), the tail and head, and the hydrophilic particles. In this case, the definition of the "interface" is the region inside $\pm 3\sigma_0$ at the averaged center of mass of the membrane.) In these figures, the red line shows the results of the LC-confined case, whereas the blue and green lines show that of the oil-confined case (The colors in the oil-confined cases are different in the number of the oil particles; $N_{\rm o} = 6400$ for the blue line, and $N_{\rm o} = 12800$ for the green line.). The system area, the interfacial tension, and the bending rigidity in the oil-confined system is defined as $A_{\rm o}$, $\gamma_{\rm eff,o}$, and $K_{\rm eff,o}$, respectively.

When $\epsilon_{1,3}$ is changed from $1.0\epsilon_0$ to $1.75\epsilon_0$, $\epsilon_{\rm I}$ is changed approximately from $-2.41\epsilon_0$ to $-2.46\epsilon_0$ as you can understand from Fig.3.8. Then, we can compare these results in such region (We call "comparable $\epsilon_{\rm I}$ region".). According to these figures, similar behaviors are confirmed: $A_{\rm o}$ becomes larger, $\gamma_{\rm eff,o}$ and $K_{\rm eff,o}$ becomes smaller by increasing the absolute value of $\epsilon_{\rm I}$ (see from the right to the left side in the horizontal axis in Fig.3.8). In the comparable $\epsilon_{\rm I}$ region, (i) $A_{\rm o}$ is first smaller than $A_{\rm m}$ (area in the LC-confined case), (ii) $\gamma_{\rm eff,o}$ and $K_{\rm eff,o}$ are both larger than those in the LC-confined system. These values in the oil-confined case rapidly approach the respective values in the LC-confined case by increasing $|\epsilon_{\rm I}|$. Why are these behaviors

in the oil-confined case qualitatively the same as but quantitatively different from those in the LC-confined case? We again consider the penetration of the oil particles into the membrane. The difference of the sizes and the shapes between the oil and the LC particle may be important for the behaviors of $A_{\rm o}$, $\gamma_{\rm eff,o}$ and $K_{\rm eff,o}$.

The simple fluid composed by the spherical particles is "softer" than the slightly complex fluid as the LC material (The word "soft" for the simple fluid means that the shape of a container to confine the simple fluid can be chosen freely: when the LC material is confined into a container and interacts with the wall of the container, that is, the anchoring is worked, a restoring force to avoid the elastic penalty of the LC material may be worked on the wall of the container by changing the shape of the container.). Then, as the oil particles penetrates into the membrane, the membrane may be softer than the "pure" membrane composed only by the surfactant or the LC-penetrating membrane. Since the oil particle is smaller than the LC particle and the surfactant molecule (the size of the oil particle is the same as the size of the tail particle of the surfactant molecule), the oil particle-penetration into the membrane easily occurs. The more the oil particles penetrate into the membrane, the larger the area of the membrane becomes. Moreover, since the oil particle is spherical, the loss of entropy of translation due to the penetration is smaller than the case of the LC particle: since the LC particle is elliptical and the penetrating LC particles tend to orient into the planar direction along the membrane due to the anisotropic interaction ($\xi > 1$), the behaviors of the LC particles, the translation and the rotation, into the membrane is strongly restricted by the surrounding surfactant molecules. Note that (i) the oil particles into the membrane lose the translational entropy rather than the oils in the bulk region and (ii) the larger $\epsilon_{1,3}$ is, the more the surfactant molecules are constrained to be around the oil particles due to the realization of the potential minimum. However, smaller size of the oil particle and "softer" property as the simple fluid compared to the LC material make the membrane be softer.

The area of the membrane can change without the penetration of the confined particles. Let us consider the case that the membrane composed of the surfactants and the confined material merely contact each other and construct their interface without the penetration. When the interaction energy between them (We will call "contact attractive energy") is strengthened attractively, the membrane area expands in order to become energetically stabler by increasing the area where both materials constructing the inter-

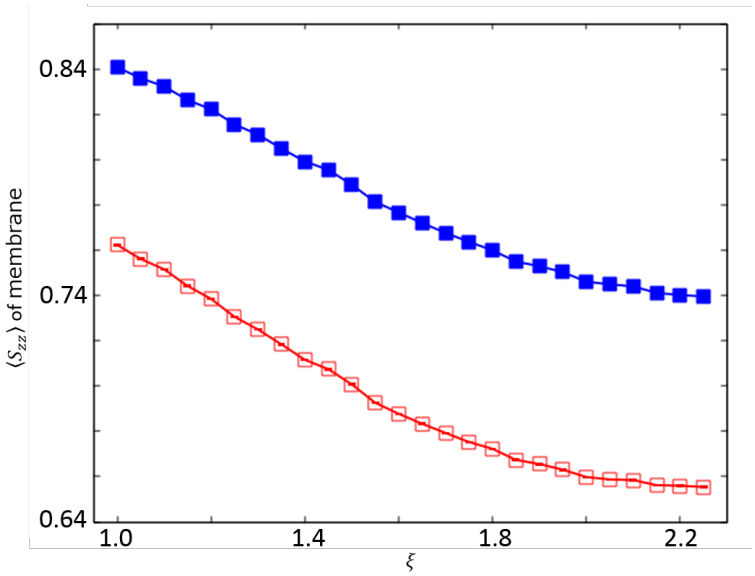

Fig. 3.9: The graphs of the order parameters of the orientation of the surfactant molecule in the LC-confined system. The red line shows the orientation order of the tail-to-head (end-to-end) vector, whereas the blue one shows that of the tail-to-tail vector.

face interact with each other. Of course the larger the membrane area is, the more the loss of the interaction energy between the surfactant molecules becomes. Then such expansion is governed also by the surfactants. In our parameter region $1.0 \leq \xi \leq 2.2$ or $-2.15 < \epsilon_{\mathrm{I}} < -2.55$, the membrane seems not to break its form, not to undergo a phase transition, and not to separate two or more parts. According to Fig.3.9, where the orientation order of the surfactant molecule in the LC-confined system is shown, there is no non-monotonic change (The red line shows the orientation order of the tail-to-head (end-to-end) vector, whereas the blue one shows that of the tail-to-tail vector. The estimation of these order parameters is performed by the same method as the estimation of that in the LC-confined system). If the disorganization or the phase transition into the membrane occurred, some changes in these orientation orders would be observed. These values gradually decreases, so that these decreases are originated from the expansion of the membrane area (The larger the membrane area is, the larger the occupied area of a single surfactant molecule becomes, then the orientation direction

of the surfactant easily changes). Therefore, in our parameter region, the membrane area expands retaining its structure by increasing the contact attractive energy (The membrane in the oil-confined system would also behave in the same manner.).

In the oil-confined system, since the area expansion of the membrane by increasing $\epsilon_{\rm I}$ occurs due to both the increase in the contact attractive energy and the penetration of the oil particles into the membrane, the area expansion is more rapid than that in the LC-confined system. In addition, the changes in $A_{\rm m}$, $\gamma_{\rm eff}$ and $K_{\rm eff}$ in the LC-confined system is originated from other effects than the penetration, so that these slopes of the changes are different from those in the oil-confined case. As a reason of these behaviors in the LC-confined system, we consider the effects of the orientation of the LC material due to the anchoring as follows.

The decreasing of $\gamma_{\rm eff}$ (Fig.3.1) with increasing ξ is interpreted as follows. Increasing the value of ξ, the depth of the interaction potential between the LC molecule and the tail particle of the surfactant is increased depending on their configuration with respect to the orientation of the LC particle to the spherical one (see Fig.2.2). In this case, the area of the membrane expands discussed above. The larger the membrane area is, the more its area fluctuates (In the case that the large area of the membrane is energetically advantageous, the membrane tends to behave as taking larger area). Then, $\gamma_{\rm eff}$ decreases. Such a decrease in the interfacial tension can be observed not only in the LC confined system but also in spherical particles confined system merely by increasing the attractive interaction energy. In the LC-confined system, the effect of the orientation of the LC particles appears. When ξ increases, the fluctuation of the interaction energy originating from the thermal fluctuation of the LC orientation also increases (See Fig.2.2. When the orientation direction of the LC particle to the spherical one changes, the interaction energy also changes. The energy change becomes larger by increasing ξ even if the same degree of the orientation change occurs.). The larger the fluctuation of the interaction energy is, the larger the fluctuation of the area of the membrane becomes since the membrane area is determined by the LC-surfactant interaction. In this case, since the membrane becomes softer with respect to the expansion of its area, $\gamma_{\rm eff}$ also decreases. The nematic order at the interface strengthens the effect of the orientational fluctuation for $\gamma_{\rm eff}$. If the LC is in the isotropic phase at the interface, the fluctuation of the local interaction energy between the surfactants and the LCs is small irrespective of the interfacial shape because the interface does not affect the distribution

of the molecular axis vectors of the LC. In this case, $\gamma_{\rm eff}$ is unchanged.

Note that the decreasing of the interfacial tension is different from the analytical result by Rey [39] because the orientational order in our case can fluctuate while that in the system discussed in ref.[39] cannot fluctuate. Such a difference in the orientation behavior is attributed to the elastic property of the LC, which can affect the membrane properties through the anchoring.

When $\xi > 1$, in our case, the LC orientation averaged over the interfacial region is directed to the averaged interfacial normal direction due to the anchoring as is shown in Fig.3.4. Such an orientational direction does not in general coincide with the natural direction of the LC determined by its elasticity. Then the local LC directions near the interface are determined by the competition between the contribution of the LC elasticity and that of the anchoring, which leads to a renormalization of the effective bending rigidity. Such a competition leads to two different regimes in the anchoring strength separated at a certain threshold value $\xi = \xi_{\rm m}$.

The bending rigidity $K_{\rm eff}$ in Fig.3.2 shows a nonmonotonic behavior as a function of the anchoring parameter ξ. As increasing ξ, first $K_{\rm eff}$ slightly increases and then decreases across the threshold value $\xi = \xi_{\rm m}$. When the anchoring effect is small compared to the LC elasticity, i.e. $1 < \xi < \xi_{\rm m}$, the local LC director near the interface does not fit to the local membrane normal due to the LC elasticity, which avoids a spatial variation of the LC directors. Then, most of the LC directors are oriented to the same direction, i.e. the *average* normal direction of the membrane, resulting in the development of the nematic layer. In this case, when the membrane fluctuates, the mismatch between the local membrane normal and the LC director imposes a penalty for the anchoring interaction, resulting in an increase in the effective bending rigidity.

Contrary to the above weak anchoring case, the behavior changes when $\xi > \xi_{\rm m}$, i.e. a strong anchoring case. In this case, the bending rigidity changes its dependence on ξ from increasing to decreasing behaviors. If the effect of the homeotropic anchoring is strong enough, the local LC directors near the membrane tend to orient to the local membrane normal. Then, the LC orientation near the interface is distorted when the membrane fluctuates, which leads to an increase in the penalty due to the LC elasticity. To suppress this elastic penalty of LC, the LC molecules just at the interface, where the LC molecules have a contact with the surfactant on the membrane, change its direction from the average membrane normal to the lateral direction along the membrane. In this case, when the membrane fluctuates in the

direction perpendicular to the LC orientation in the lateral plane, the LC elastic penalty is not imposed, and the bending rigidity of the membrane effectively decreases. Such a change in the LC orientation from the membrane normal to the lateral direction of the membrane is realized by the so-called " depletion effect " which originates from the entropic effect with respect to the steric hindrance on the translation of the LC molecules just at the interface. The change in the LC orientation at the interface is confirmed by the orientation order parameter of the LC near the membrane which shows the similar behavior to the bending rigidity (see $S_{\rm int}$ in Fig.3.4), that is, the order changes its tendency from increasing to decreasing behavior. Note that the LC molecules slightly away from the membrane (but near the interface) retain the orientation in z-direction by the anchoring interaction whose interaction range corresponds to the size of the long axis of the LC particle. Then the effect of the anchoring remains at least within a few molecular layers of LC even if the LC orientations are mixed (z and $x-y$ orientation) near the interface.

This orientational behavior of the LC can be realized due to the weak nematic in the bulk region. If the bulk LC is in the nematic phase, the membrane fluctuation can be transfered into the bulk region, resulting in the higher penalty from the LC elasticity than that in our case.

Next we try to consider how the orientational effect is important to the interfacial tension and bending rigidity by analyzing the free energy model including the orientational anchoring of the LC material in the interfacial energy part as is described in the next section.

3.2 Analyzing free energy with orientational anchoring

In this section, we consider some conditions, where the variations of the total free energy for the order parameter of the LC material and for the position of the component of the membrane get 0, to minimize the total free energy in the LC-confined system with the orientational anchoring. Since the membrane properties at the equilibrium state can be characterized by the minimized free energy, we expect to derive the important information from such analysis. The bulk LC property corresponds to the weak nematic one, but at interface nematic order appears due to the anchoring by the membrane. Since the LC

material is elastic, the nematic order decreases gradually from the interface region to the bulk region. In this case, it is important for the free energy minimization to consider both the interfacial energy and the bulk one because the LC material and the membrane are elastic and mutually interact through the anchoring, that is, the bulk LC property affects the membrane. Then the total free energy in such system is written in the continuum model as,

$$F_{\rm tot} = \int_{\rm V} dV \left(f_0 + f_{\rm el}\right) + \int_{\rm A} dA \left(\gamma + \frac{K}{2}H^2 + \frac{\gamma_{\rm a}}{2}\boldsymbol{g}_3\boldsymbol{g}_3 : \boldsymbol{Q}\right) + P\left[\int_{\rm V} dV - V_0\right], \tag{3.4}$$

where f_0 is the local free energy of the LC material and $f_{\rm el}$ is the elastic energy, both written in terms of the tensor order parameter $\boldsymbol{Q}$ introduced in Sec.1.1.1, P the pressure and V_0 the equilibrium volume of the system. Although the hydrophilic fluid exists outside the membrane in our simulation, the LC material has the orientational elasticity (and the local ordered energy) so that the influence from the hydrophilic (simple) fluid can be neglected. H is the mean curvature of the membrane, and since the membrane is almost planar in this system, the spontaneous curvature is zero. γ and K are the interfacial tension and the bending rigidity, which include the effects of the penetration of the particles into the membrane. Since we focus on the orientational effect due to the anchoring, we assume that γ and K are independet of the LC order parameter, although they depend on ξ of the anchoring parameter in above simulation. $\gamma_{\rm a}$ in Eq.3.4 corresponds to the strength of the anchoring in the continuum model, and we assumed $\gamma_{\rm a} = \gamma_{\rm a}(\xi)$.

Here, in the equilibrium state, since the total force is zero at any point in the system, we consider the balance of the forces working on the interface including the bulk energy contribution. Although a force is worked on a point in the bulk region, we focus on the forces inducing the deformation of the membrane.

Assuming that a point $\boldsymbol{r}$ in a material is deformed by a displacement vector $\boldsymbol{u}(\boldsymbol{r})$, the virtual work at $\boldsymbol{r}$ is written by $\delta w = -\boldsymbol{f}\cdot\boldsymbol{u}$, where $\boldsymbol{f}$ is the restoring force acting on $\boldsymbol{r}$. When the system deviates from an equilibrium state by the deformation $\boldsymbol{u}(\boldsymbol{r})$, the force $\boldsymbol{f}$ is generaged to restore the system to equilibrium state. Then, in equilibrium state, since $\delta w = 0$ is realized for any $\boldsymbol{u}(\boldsymbol{r})$, $\boldsymbol{f} = \boldsymbol{0}$ is the equilibrium condition. Then we try to derive the restoring force working on the interface.

Deforming the position of the membrane $\boldsymbol{R}$ by a displacement $\boldsymbol{u}$, a new position after the deformation is written as $\boldsymbol{R}' = \boldsymbol{R} + \boldsymbol{u}$. In this case, the

area element and the curvature as the geometric values of the membrane changes by the displacement. To obtain these changed values, we calculate the geometric vectors on the deformed membrane as follows,

$$\boldsymbol{g}'_1 = \frac{\partial \boldsymbol{R}'}{\partial x} = \boldsymbol{g}_1 + \boldsymbol{u}_{,x}, \quad \boldsymbol{g}'_2 = \frac{\partial \boldsymbol{R}'}{\partial y} = \boldsymbol{g}_2 + \boldsymbol{u}_{,y}, \quad \boldsymbol{g}'_3 = \frac{\boldsymbol{g}'_1 \times \boldsymbol{g}'_2}{|\boldsymbol{g}'_1 \times \boldsymbol{g}'_2|}, \tag{3.5}$$

where all values with prime $(\cdot)'$ are the changed ones by the displacement $\boldsymbol{u}$. $\boldsymbol{g}_1$ and $\boldsymbol{g}_2$ are the original tangential vectors on the membrane along the curvilinear coordinates, where $\boldsymbol{u}_{,\alpha}$ means the difference in α-direction. $|\boldsymbol{g}'_1 \times \boldsymbol{g}'_2| = \sqrt{d'_g}$ which is the area element after the deformation, $d'_g = \det |m'_{\alpha\beta}|$, and $m'_{\alpha\beta} = \boldsymbol{g}'_\alpha \cdot \boldsymbol{g}'_\beta$ is the metric tensor on the membrane after the deformation. Using these 3 deformed vectors, the second fundamental form after the deformation is calculated as $f'_{\alpha\beta} = (\partial \boldsymbol{g}'_\alpha / \partial x_\beta) \cdot \boldsymbol{g}'_3$, $x_\beta = x, y$. Then the mean curvature of the deformed surface is calculated up to the second order in $h(x, y)$ of the membrane height at (x, y) and the first order for the displacement $\boldsymbol{u}$ (we assume the small deformation around the equilibrium state), as follows,

$$\begin{aligned} H' \approx H + d_g^{-\frac{3}{2}} \big\{ & (-2h_{,xx} + 3h_{,yy})u^x_{,x} + (3h_{,xx} - 2h_{,yy})u^y_{,y} - 2h_{,xy}(u^x_{,y} + u^y_{,x}) \\ & - h_{,x}u^x_{,xx} - h_{,x}u^x_{,yy} - h_{,y}u^y_{,xx} - h_{,y}u^y_{,yy} + 2(h_{,x}h_{,yy} - h_{,y}h_{,xy})u^z_{,x} \\ & + 2(h_{,y}h_{,xx} - h_{,x}h_{xy})u^z_{,y} + (1 + h^2_{,y})u^z_{,xx} + (1 + h^2_{,x})u^z_{,yy} + 2h_{,x}h_{,y}u^z_{,xy} \big\}, \end{aligned} \tag{3.6}$$

where u^α is the α component of the displacement vector $\boldsymbol{u}$. Since the membrane we are considering is almost planar, the term with the 0'th order of u^α does not exist. As the contribution from the curvature to the virtual work is important, the term with the 2nd order of u^α is retained in Eq.3.6. The deformed area element $\sqrt{d'_g}$ can be written as

$$\sqrt{d'_g} \approx \sqrt{d_g} + d_g^{-\frac{1}{2}} \left\{ (1 + h^2_{,y})u^x_{,x} + (1 + h^2_{,x})u^y_{,y} - h_{,x}h_{,y}(u^x_{,y} + u^y_{,x}) + h_{,x}u^z_{,x} + h_{,y}u^z_{,y} \right\}, \tag{3.7}$$

then we can calculate the interfacial free energy F'_{A} for the deformed state.

On the other hand, we can derive some contributions from the bulk free energy to the virtual work. A point $\boldsymbol{r}$ is changed for $\boldsymbol{r}' = \boldsymbol{r} + \boldsymbol{u}$, the derivative for $\boldsymbol{Q}$ is changed as follows,

$$\frac{\partial \boldsymbol{Q}'}{\partial \boldsymbol{r}'} = \frac{\partial \boldsymbol{Q}'}{\partial \boldsymbol{r}} \cdot \frac{\partial \boldsymbol{r}}{\partial \boldsymbol{r}'} \approx \frac{\partial \boldsymbol{Q}}{\partial \boldsymbol{r}} \cdot \left(\mathbf{1} - \frac{\partial \boldsymbol{u}}{\partial \boldsymbol{r}} \right). \tag{3.8}$$

In Eq.3.8, we used $\boldsymbol{r} = \boldsymbol{r}' - \boldsymbol{u}$ and assumed the small distortion, $(\partial \boldsymbol{u}/\partial \boldsymbol{r}') \approx (\partial \boldsymbol{u}/\partial \boldsymbol{r})$ at the last line. Here, although $\boldsymbol{Q}$ may be changed to $\boldsymbol{Q}'$ by the displacement as written in the first line of Eq.3.8, we assumed $\boldsymbol{Q}' \approx \boldsymbol{Q}$ in the last line of Eq.3.8 since the local change in $\boldsymbol{Q}$ is small enough to ignore its contribution to the change in the elastic term. Considering the change in the volume, $d\boldsymbol{r}' = \det|\partial \boldsymbol{r}'/\partial \boldsymbol{r}| d\boldsymbol{r} \approx (1 + Tr(\partial \boldsymbol{u}/\partial \boldsymbol{r}))d\boldsymbol{r}$, we can calculate the bulk free energy F'_{V} for the deformed state.

Since the system has the degree of freedom of the LC tensor order parameter $\boldsymbol{Q}$, we next consider the variation of the free energy by that of $\boldsymbol{Q}$, which is defined as $\boldsymbol{C}(\boldsymbol{r}) = \delta F_{\mathrm{tot}}/\delta \boldsymbol{Q}$. Variation of the total free energy for only the small deviation of $\boldsymbol{Q}$ denoted as $\delta \boldsymbol{Q}$ is given by

$$\begin{aligned} \delta F_{\mathrm{tot,forQ}} = & \int_{\mathrm{V}} dV \left(A(T)\boldsymbol{Q} + B\boldsymbol{Q}\cdot\boldsymbol{Q} + C\boldsymbol{Q}:\boldsymbol{Q}\boldsymbol{Q} - L_2\boldsymbol{\nabla}^2\boldsymbol{Q} \right) : \delta\boldsymbol{Q} \\ & + \int_{\mathrm{A}} dA \left(\gamma_{\mathrm{a}}\boldsymbol{g}_3\boldsymbol{g}_3 + L_2\boldsymbol{g}_3\cdot\boldsymbol{\nabla}\boldsymbol{Q} \right) : \delta\boldsymbol{Q}, \end{aligned} \tag{3.9}$$

where the coefficient of $\delta \boldsymbol{Q}$ in the 1st term corresponds to the bulk force working at $\boldsymbol{r}$ defined as

$$\boldsymbol{C}_{\mathrm{lc,b}} = A(T)\boldsymbol{Q} + B\boldsymbol{Q}\cdot\boldsymbol{Q} + C\boldsymbol{Q}:\boldsymbol{Q}\boldsymbol{Q} - L_2\boldsymbol{\nabla}^2\boldsymbol{Q}. \tag{3.10}$$

The LC orientational force contribution on the interface is defined in the second term of Eq.3.9 as

$$\boldsymbol{C}_{\mathrm{lc,int}} = \gamma_{\mathrm{a}}\boldsymbol{g}_3\boldsymbol{g}_3 + L_2\boldsymbol{g}_3\cdot\boldsymbol{\nabla}\boldsymbol{Q}. \tag{3.11}$$

From this definition, it can be understood that the interfacial anchoring also affects the bulk properties of the LC phase through the orientational force in the boundary condition. In Eq.3.9, for simlicity, we took only the L_2 term from Eq.1.13 in Sec.1.1.1 .

Therefore, using these contributions from the restoring force for the positional displacement and the LC orientational force on the interface, we can

derive the modified (by the orientational force) restoring force as follows:

$$
\begin{aligned}
F_x \approx & \sqrt{d_g}(f_0 + f_{\rm el})h_{,x} - \gamma h_{,x}\tilde{H} + Kh_{,x}(\tilde{H}_{,xx} + \tilde{H}_{,yy}) \\
& - \frac{\gamma_{\rm a}}{2}\{((3h_{,x}h_{,xx} + 4h_{,y}h_{,xy} - h_{,x}h_{,yy})\boldsymbol{e}_z\boldsymbol{e}_z + 2h_{,x}(h_{,xx}\boldsymbol{e}_x\boldsymbol{e}_x + h_{,yy}\boldsymbol{e}_y\boldsymbol{e}_y) \\
& + 2h_{,x}h_{,xy}(\boldsymbol{e}_x\boldsymbol{e}_y + \boldsymbol{e}_y\boldsymbol{e}_x)) : \boldsymbol{Q} - h_{,x}(\boldsymbol{e}_x\boldsymbol{e}_z + \boldsymbol{e}_z\boldsymbol{e}_x) : \boldsymbol{Q}_{,x} - h_{,x}(\boldsymbol{e}_y\boldsymbol{e}_z + \boldsymbol{e}_z\boldsymbol{e}_y) : \boldsymbol{Q}_y\} \\
& + \sqrt{d_g}Ph_{,x}, \qquad (3.12) \\
F_y \approx & \sqrt{d_g}(f_0 + f_{\rm el})h_{,y} - \gamma h_{,y}\tilde{H} + Kh_{,y}(\tilde{H}_{,xx} + \tilde{H}_{,yy}) \\
& - \frac{\gamma_{\rm a}}{2}\{((3h_{,y}h_{,yy} + 4h_{,x}h_{,xy} - h_{,y}h_{,xx})\boldsymbol{e}_z\boldsymbol{e}_z + 2h_{,y}(h_{,xx}\boldsymbol{e}_x\boldsymbol{e}_x + h_{,yy}\boldsymbol{e}_y\boldsymbol{e}_y) \\
& + 2h_{,y}h_{,xy}(\boldsymbol{e}_x\boldsymbol{e}_y + \boldsymbol{e}_y\boldsymbol{e}_x)) : \boldsymbol{Q} - h_{,y}(\boldsymbol{e}_x\boldsymbol{e}_z + \boldsymbol{e}_z\boldsymbol{e}_x) : \boldsymbol{Q}_{,x} - h_{,y}(\boldsymbol{e}_y\boldsymbol{e}_z + \boldsymbol{e}_z\boldsymbol{e}_y) : \boldsymbol{Q}_y\} \\
& + \sqrt{d_g}Ph_{,y}, \qquad (3.13) \\
F_z \approx & -(f_0 + f_{\rm el}) + \gamma\tilde{H} - K(\tilde{H}_{,xx} + \tilde{H}_{,yy}) \\
& + \frac{\gamma_{\rm a}}{2}\left\{\left(2(h_{,xx}\boldsymbol{e}_x\boldsymbol{e}_x + h_{,xy}(\boldsymbol{e}_x\boldsymbol{e}_y + \boldsymbol{e}_y\boldsymbol{e}_x) + h_{,yy}\boldsymbol{e}_y\boldsymbol{e}_y) - \tilde{H}\boldsymbol{e}_z\boldsymbol{e}_z\right) : \boldsymbol{Q}\right. \\
& \left. -(\boldsymbol{e}_x\boldsymbol{e}_z + \boldsymbol{e}_z\boldsymbol{e}_x) : \boldsymbol{Q}_{,x} - (\boldsymbol{e}_y\boldsymbol{e}_z + \boldsymbol{e}_z\boldsymbol{e}_y) : \boldsymbol{Q}_{,y} - \boldsymbol{e}_z\boldsymbol{e}_z : \boldsymbol{Q}_{,z}\right\} \\
& + \frac{\gamma_{\rm a}}{2}\{((3h_{,x}h_{,xx} + 2h_{,y}h_{,xy} + h_{,x}h_{,yy})(\boldsymbol{e}_x\boldsymbol{e}_z + \boldsymbol{e}_z\boldsymbol{e}_x) \\
& + (3h_{,y}h_{,yy} + 2h_{,x}h_{,xy} + h, yh_{,xx})(\boldsymbol{e}_y\boldsymbol{e}_z + \boldsymbol{e}_z\boldsymbol{e}_y)) : \boldsymbol{Q} \\
& + (2h_{,x}\boldsymbol{e}_x\boldsymbol{e}_x + h_{,y}(\boldsymbol{e}_x\boldsymbol{e}_y + \boldsymbol{e}_y\boldsymbol{e}_x) - h_{,x}\boldsymbol{e}_z\boldsymbol{e}_z) : \boldsymbol{Q}_{,x} \\
& + (2h_{,y}\boldsymbol{e}_y\boldsymbol{e}_y + h_{,x}(\boldsymbol{e}_x\boldsymbol{e}_y + \boldsymbol{e}_y\boldsymbol{e}_x) - h_{,y}\boldsymbol{e}_z\boldsymbol{e}_z) : \boldsymbol{Q}_{,y} \\
& + (h_{,x}(\boldsymbol{e}_x\boldsymbol{e}_z + \boldsymbol{e}_z\boldsymbol{e}_x) + h_{,y}(\boldsymbol{e}_y\boldsymbol{e}_z + \boldsymbol{e}_z\boldsymbol{e}_y) : \boldsymbol{Q}_{,z}\} - P, \qquad (3.14)
\end{aligned}
$$

where $\tilde{H} = h_{,xx} + h_{,yy}$. F_x and F_y in Eq.3.12 are symmetric with respect to the exchange of the coordinates $x \leftrightarrow y$. In the system considered here, since i) the membrane is almost planar, ii) the LC material is weak nematic in the bulk region, and iii) the anchoring condition is homeotropic, then the restoring forces are symmetric in (x, y) plane (if the anchoring condition is the planar orientation and the LC material is uniaxial in the planar direction, the system may have an asymmetry in (x, y) plane due to the anisotropic fluctuation of the LC orientation).As can be see from Eq.3.12, an expansion and a bending of the membrane are coupled with the orientational order and its gradient of the LC material at the interface. As solving the following equations

$$
\boldsymbol{C}_{\rm lc,b} = \boldsymbol{C}_{\rm lc,int} = \boldsymbol{F} = \boldsymbol{0}, \qquad (3.15)
$$

as the boundary condition, we may get the equilibrium states for the LC and the membrane.

Since we have the idea that the LC and the membrane mutually interact through the boundary conditions, we again try to analyze the results of our simulation constructing the free energy in such system including some effective energy terms expressing above boundary conditions, as following section.

3.3 Analyzing free energy including some effective terms

3.3.1 Constructing free energy model

As we derived above, the LC material couples the deformation of the membrane through the anchoring interaction. In addition, as can be seen from our simulation results, the bending rigidity $K_{\rm eff}$ increases at lower ξ region, which may be due to the simultaneous increase in the order parameter of the LC at (just) interface (see Fig.3.2 and the blue line in Fig.3.4). If the consideration is valid, the initial increase in $K_{\rm eff}$ is caused by the growth of the nematic layer which is elastically "rigid". According to Fig.3.4, the "maximum order" $S_{\rm max}$ shown by the red line continues to increase up to $\xi \sim 2.0$ at least, whereas $S_{\rm int}$ changes its tendency from the increasing to the decreasing behavior. Although the point in the z-direction where $S_{\rm max}$ can be observed is slightly away from the "just" interface, the behavior of $S_{\rm max}$ also affects the membrane as well as the just interfacial order, $S_{\rm int}$. Then, we assume that the rigidity of the membrane is affected by the growth of the nematic layer.

We can construct the following model free energy,

$$
\begin{aligned}
F = &\int_0^{L_x}\int_0^{L_y}\int_{-z_0}^{z_0} d\boldsymbol{r}\left\{\frac{A}{2}Q_{\alpha\beta}Q_{\alpha\beta} + \frac{L_2}{2}\partial_\alpha Q_{\beta\gamma}\partial_\alpha Q_{\beta\gamma}\right\} \\
&+ \int_0^{L_x}\int_0^{L_y} d\boldsymbol{a}\left\{\gamma + \frac{K}{2}(\partial_\alpha m_\alpha)^2 + \frac{\gamma_{\rm a}}{2}m_\alpha Q_{\alpha\beta}m_\beta + K_{\rm a}m_\alpha\partial_\beta m_\gamma\partial_\alpha Q_{\beta\gamma}\right. \\
&\left. + \frac{K_{\rm b}}{4}m_\alpha Q_{\alpha\beta}m_\beta(\partial_\gamma m_\gamma)^2\right\}\Big|_{\pm z_0}, \qquad (3.16)
\end{aligned}
$$

where L_x, L_y are respectively the size in x- and y-direction of our simulation

box, and $\pm z_0$ is not the size of the simulation box but the averaged position of the almost planar membrane on the z-axis. Although the actual membrane height $h(x, y)$ should be set as the integral region in the z-direction, we set the averaged membrane position for simplicity. $d\boldsymbol{a}$ is the area element mentioned in Sec.1.2.2. We construct the free energy Eq.3.16 up to the 2nd order terms for the bulk part, and the curvature is expressed by $H \approx \partial_\alpha m_\alpha$, where m_α is the α component of the normal vector of the membrane expressed by $\boldsymbol{g}_3$ in Sec.3.2. Here, the additional terms mean the following: the K_a term shows the elastic coupling effect between the LC material and the membrane, and the K_b term shows the effect of the nematic layer, which directly affects the coefficient of the curvature energy of the membrane. These terms can be obtained from the result of the expansions for the following free energy of the membrane,

$$f_{\mathrm{mem},0} = c_0 + c_{1,\alpha} m_\alpha + c_{2,\alpha\beta} m_\alpha m_\beta + d_{3,\alpha\beta} \partial_\alpha m_\beta + d_{4,\alpha\beta\alpha'\beta'} \partial_\alpha m_\beta \partial_{\alpha'} m_{\beta'}, \tag{3.17}$$

which is expanded by the membrane normal m_α and its gradient $\partial_\alpha m_\beta$. If the membrane is in a vacuum, the constant and the 2nd power of the gradient terms are merely remained for some conditions, $|\boldsymbol{m}| = 1$ and the spatial-inversion symmetry onto the membrane surface. In our simulation, since the membrane is put on the surface of the LC material (and simultaneously contacts with the hidrophilic isotropic fluid, but it is omitted now), these coefficients in Eq.3.17 are dependent on some values of the LC material, the tensor order parameter and its gradient. Thus, assuming the following expansion for these coefficients,

$$c_{2,\alpha\beta} \approx c_{2,0} \delta_{\alpha\beta} + \frac{\gamma_\mathrm{a}}{2} Q_{\alpha\beta}, \tag{3.18}$$

$$d_{3,\alpha\beta} \approx K_\mathrm{a} m_\gamma \partial_\gamma Q_{\alpha\beta}, \tag{3.19}$$

$$d_{4,\alpha\beta\alpha'\beta'} \approx \delta_{\alpha\beta}\delta_{\alpha'\beta'} \left(\frac{K}{2} + \frac{K_\mathrm{b}}{4} m_\gamma m_\eta Q_{\gamma\eta} \right), \tag{3.20}$$

$$c_0 + c_{2,0} = \gamma, \tag{3.21}$$

we can get the above model free energy Eq.3.16. Note that although other kinds of the expansions are considered, they give the similar form in Eq.3.16, or may give some different forms but now omitted for simplicity, and some is vanished by the spatial inversion symmetry. As same as in Eq.3.4, the coefficients γ and K of the membrane do not depend on the anchoring parameter

ξ in our simulation, while $\gamma_{\rm a}$, $K_{\rm a}$ are assumed to depend on ξ. However, $K_{\rm b}$ does not depend on ξ in order to assume that $K_{\rm b}$ term shows the effect of the elastic property of the nematic layer (then $K_{\rm b}$ can depend on the elastic property of the LC material). In this case, $K_{\rm b}$ may depend on the potential parameter κ' in Eq.2.3 which changes the elastic properties of the LC material.

Because the constructed free energy Eq.3.16 has some assumptions mentioned above, this may be qualitatively valid but not quantitatively for our simulation results. To adjust this analysis with respect to the dimension to our simulation setting, we define the dimensionless coefficients as follows. The coordinate variables are written as $(x, y, z) = \sigma_0(x^*, y^*, z^*)$, and the z component of the surfactant position is $h(x, y) = \sigma_0 h^*$, and $F = \epsilon_0 F^*$. Other parameters are changed as following, $\gamma = (\epsilon_0/\sigma_0^2)\gamma^*$, $K = \epsilon_0 K^*$, $\gamma_{\rm a} = (\epsilon_0/\sigma_0^2)\gamma_{\rm a}^*$, $K_{\rm a} = \epsilon_0 K_{\rm a}^*$, and $K_{\rm b} = \epsilon_0 K_{\rm b}^*$. The system size parameters are changed as $(L_x, L_y, z_0) = \sigma_0(L_x^*, L_y^*, z_0^*)$ and omitting superscript $(\cdot)^*$ in the same way in the material parameters.

In general, $Q_{\alpha\beta}(\boldsymbol{r})$ is defined as $Q_{\alpha\beta}(\boldsymbol{r}) = \langle \boldsymbol{u}_\alpha \boldsymbol{u}_\beta - \delta_{\alpha\beta}/3 \rangle$ as mentioned in Sec.1.1.1, where u_α is the α-component of the molecular director of the LC material. In our simulation, since the state of the bulk LC is nearly isotropic, $Q_{\alpha\beta}(\boldsymbol{r})$ is small. However, in the vicinity of the membrane, it is expected that $\langle u_\alpha u_\beta \rangle \approx \langle m_\alpha m_\beta \rangle$ due to the effect of the anchoring. Thus we write $Q_{\alpha\beta}(\boldsymbol{r})$ by two forms in equilibrium state as follows;

$$\boldsymbol{Q}(-z_0 < z < z_0) = \frac{3}{2} S(\boldsymbol{r})(\boldsymbol{n}(\boldsymbol{r})\boldsymbol{n}(\boldsymbol{r}) - \frac{\mathbf{1}}{3}), \tag{3.22}$$

$$\boldsymbol{Q}(z = \pm z_0) = \frac{3}{2} S(\boldsymbol{r})(\boldsymbol{m}(\boldsymbol{r})\boldsymbol{m}(\boldsymbol{r}) - \frac{\mathbf{1}}{3}), \tag{3.23}$$

where n_α is the local director and $S(\boldsymbol{r})$ is the local scalar order parameter of the LC. In the bulk region, since the correlation in the LC directors is very small due to the nearly isotropy of the LC material, we assume that the elastic contribution from the gradient terms of n_α to the bluk free energy can be neglected (Using this assumption, the bulk free energy can be written only by the scalar order parameter $S(\boldsymbol{r})$ and its gradient). In these expressions, $S(\boldsymbol{r})$, n_α, and m_α are the local averaged values.

Since the membrane shows the planar form averagely, m_α is written as follows,

$$\boldsymbol{m}(x, y) = (-\partial_x h(x, y), -\partial_y h(x, y), 1 - \frac{1}{2}|\boldsymbol{\nabla} h(x, y)|^2). \tag{3.24}$$

Then rewriting the free energy using these expressions for the order parameters, which we assumed to be small deformation of membrane, $|\boldsymbol{\nabla} h| \ll 1$, and $d\boldsymbol{a} = \sqrt{1+|\boldsymbol{\nabla} h|^2}dxdy \approx (1+|\boldsymbol{\nabla} h|^2/2)dxdy$, the free energy is rewritten as follows,

$$
\begin{aligned}
F = & \frac{3}{4}\int d\boldsymbol{r}\left\{AS(\boldsymbol{r})^2 + L_2|\boldsymbol{\nabla} S(\boldsymbol{r})|^2\right\} \\
& + \int dxdy\left\{\frac{\gamma}{2}|\boldsymbol{\nabla}_s h(x,y)|^2 + \frac{K}{2}\left(\boldsymbol{\nabla}_s^2 h(x,y)\right)^2 + \frac{\gamma_{\mathrm{a}}}{2}\left(S(x,y,z_0)+S(x,y,-z_0)\right)\right. \\
& \times\left(1+\frac{1}{2}|\boldsymbol{\nabla}_s h(x,y)|^2\right) + \frac{K_{\mathrm{a}}}{2}\left(\partial_z S(x,y,z_0)+\partial_z S(x,y,-z_0)\right)\boldsymbol{\nabla}_s^2 h(x,y) \\
& \left.+\frac{K_{\mathrm{b}}}{4}\left(S(x,y,z_0)+S(x,y,-z_0)\right)\left(\boldsymbol{\nabla}_s^2 h(x,y)\right)^2\right\}, \qquad (3.25)
\end{aligned}
$$

where the constant terms are omitted, and $\boldsymbol{\nabla}_s = (\mathbf{1}-\boldsymbol{mm})\cdot\boldsymbol{\nabla}$ shows the tangential gradient on the membrane surface. In this free energy, since the surface gradient terms include only the 2nd order terms, $\boldsymbol{\nabla}_s \approx (\mathbf{1}-\boldsymbol{e}_z)\cdot\boldsymbol{\nabla} = (\partial_x, \partial_y, 0)$. As referred above, we neglect the n_α-dependent terms. We assume that the membrane properties are the same for both upper and lower membranes by the symmetry reason. Subsequently, this free energy model is Fourier transformed by considering the Fourier components of both order parameters, $S(\boldsymbol{r})$ and $h(x,y)$, in (x,y)-plane that is averagely parallel to the membrane,

$$S(\boldsymbol{r}) = \frac{1}{N_{\mathrm{l}}}\sum_{\boldsymbol{q}} S(\boldsymbol{q},z)\exp\left(i\boldsymbol{q}\cdot\boldsymbol{x}\right), \qquad (3.26)$$

$$h(x,y) = \frac{1}{N_{\mathrm{s}}}\sum_{\boldsymbol{q}} h(\boldsymbol{q})\exp\left(i\boldsymbol{q}\cdot\boldsymbol{x}\right), \qquad (3.27)$$

where N_{l} and N_{s} are the number of the LC and the surfactant molecules, respectively, and $\boldsymbol{x}$ and $\boldsymbol{q}$ are the position vector in (x,y)-plane and the wave vector in the Fourier space, respectively. Here, for dimensionless, $\boldsymbol{q} = (1/\sigma_0)\boldsymbol{q}^*$ and $\boldsymbol{q}^*$ is replaced to $\boldsymbol{q}$ as same as other parameters. In our simulation, z-direction is a special direction because of the existence of the two membranes. After substituting these Fourier transformed forms into Eq.3.25, minimizing the resulted form with respect to $S(\boldsymbol{q},z)$ which is conducted by assuming the system to be in the infinite system of the LC material (Considering in the LC bulk system. This assumption is valid in the case

that the bulk LC is in weak nematic or isotropic phase as in our simulation.), and solving the differential equation with respect to z, we obtain as its equilibrium form for the value of the bulk LC,

$$S(-\boldsymbol{q}, z) = C(-\boldsymbol{q}) \exp(\lambda_q z) + D(-\boldsymbol{q}) \exp(-\lambda_q z), \tag{3.28}$$

$$\lambda_q^2 = \frac{A}{L} + \boldsymbol{q}^2, \tag{3.29}$$

where $C(-\boldsymbol{q})$ and $D(-\boldsymbol{q})$ are the Fourier coefficients of $S(\boldsymbol{q}, z)$ and only depends on $\boldsymbol{q}$. The surface term is neglected because now we consider the infinite system. Substituting $S(-\boldsymbol{q}, z)$ in Eq.3.25 including the interfacial part of the free energy, we can get the mode-coupled form due to the 3rd order term with respect to the order parameters as can be seen in Eq.3.25 (the $\gamma_{\rm a}$ and the $K_{\rm b}$ terms) as following,

$$F_{\rm bulk} = \frac{3A_{\rm m}}{2N_{\rm l}} L_2 \sum_{\boldsymbol{q}} \lambda_q (|C_q|^2 + |D_q|^2) \sinh(2\lambda_q z_0), \tag{3.30}$$

$$\begin{aligned} F_{\rm int} = \frac{A_{\rm m}}{N_{\rm s}} \sum_{\boldsymbol{q}} \Bigg[& (\gamma q^2 + K q^4) |h_q|^2 + \frac{1}{N_{\rm l}} \{ \gamma_{\rm a} \cosh(\lambda_q z_0)(C_q + D_q) \\ & \left(\delta_{q,0} + \frac{1}{2} \sum_{\boldsymbol{q}_2, \boldsymbol{q}_3} \boldsymbol{q}_2 \cdot \boldsymbol{q}_3 h_{q_2} h_{-q_3} \delta_{\boldsymbol{q}+\boldsymbol{q}_2-\boldsymbol{q}_3, \boldsymbol{0}} \right) - K_{\rm a} \lambda_q (C_q - D_q) \cosh(\lambda_q z_0) q^2 h_{-q} \\ & + \frac{K_{\rm b}}{2} (C_q + D_q) \cosh \lambda_q z_0 \sum_{\boldsymbol{q}_2, \boldsymbol{q}_3} \boldsymbol{q}_2^2 \boldsymbol{q}_3^2 h_{q_2} h_{q_3} \delta_{\boldsymbol{q}+\boldsymbol{q}_2+\boldsymbol{q}_3, \boldsymbol{0}} \Bigg\} \Bigg], \end{aligned} \tag{3.31}$$

where $A_{\rm m} = L_x L_y$ is the area of the cross-section of the system in the $x - y$ plane.

Above derived free energies Eqs.3.30 and 3.31 are the effective interfacial free energy including the LC free energy, the membrane free energy, and the interaction energy between them with the bulk LC being in equilibrium state. The behaviors of the LC and the membrane at the interface are determined as minimizing the total effective free energy including Eqs.3.30 and 3.31. Now we want to get information of the membrane interacting with the LC. Since the LC material in our simulation merely has the interface and does not construct the layer forms as being in the smectic phase, it is allowed to realize more rapidly the equilibration of the LC material than the membrane.

Then, again minimizing the total free energy by C_q and D_q,

$$C_{-q} = -\frac{A_\mathrm{m}}{4N_\mathrm{l}\Gamma_\mathrm{l}\sinh(\lambda_q z_0)}\left\{\Gamma_{\mathrm{f}1}\delta_{q,0} + \Gamma_{\mathrm{f}2}\delta_{\boldsymbol{q}+\boldsymbol{q}_2-\boldsymbol{q}_3,\boldsymbol{0}} - \Gamma_{\mathrm{f}3} + \Gamma_{\mathrm{f}4}\delta_{\boldsymbol{q}+\boldsymbol{q}_2+\boldsymbol{q}_3,\boldsymbol{0}}\right\}, \tag{3.32}$$

$$D_{-q} = -\frac{A_\mathrm{m}}{4N_\mathrm{l}\Gamma_\mathrm{l}\sinh(\lambda_q z_0)}\left\{\Gamma_{\mathrm{f}1}\delta_{q,0} + \Gamma_{\mathrm{f}2}\delta_{\boldsymbol{q}+\boldsymbol{q}_2-\boldsymbol{q}_3,\boldsymbol{0}} + \Gamma_{\mathrm{f}3} + \Gamma_{\mathrm{f}4}\delta_{\boldsymbol{q}+\boldsymbol{q}_2+\boldsymbol{q}_3,\boldsymbol{0}}\right\}, \tag{3.33}$$

$$\Gamma_\mathrm{l} = \frac{3}{2}L_2\lambda_q, \tag{3.34}$$

$$\Gamma_{\mathrm{f}1} = \frac{A_\mathrm{m}}{N_\mathrm{s}}\gamma_\mathrm{a}, \tag{3.35}$$

$$\Gamma_{\mathrm{f}2} = \frac{A_\mathrm{m}}{N_\mathrm{s}}\frac{\gamma_\mathrm{a}}{2}\sum_{\boldsymbol{q}_2,\boldsymbol{q}_3}\boldsymbol{q}_2\cdot\boldsymbol{q}_3 h_{q_2}h_{-q_3}, \tag{3.36}$$

$$\Gamma_{\mathrm{f}3} = \frac{A_\mathrm{m}}{N_\mathrm{s}}K_\mathrm{a}\lambda_q q^2 h_{-q}, \tag{3.37}$$

$$\Gamma_{\mathrm{f}4} = \frac{A_\mathrm{m}}{N_\mathrm{s}}\frac{K_\mathrm{b}}{2}\sum_{\boldsymbol{q}_2,\boldsymbol{q}_3}\boldsymbol{q}_2^2\boldsymbol{q}_3^2 h_{q_2}h_{q_3}. \tag{3.38}$$

Finally substituting them into the total free energy including Eqs.3.30 and 3.31 and taking up to the 2nd order of h_q, we get

$$F = \frac{L_x L_y}{N_{\mathrm{s}^2}}\sum_{\boldsymbol{q}}\left[\left(\gamma - \frac{\gamma_\mathrm{a}^2}{\gamma_\mathrm{lc}}\right)\boldsymbol{q}^2 + \left(K - \frac{K_\mathrm{a}^2}{E_\mathrm{lc}} - \frac{\gamma_\mathrm{a}}{\gamma_\mathrm{lc}}K_\mathrm{b}\right)\boldsymbol{q}^4\right]|h_{\boldsymbol{q}}|^2, \tag{3.39}$$

where $\gamma_\mathrm{lc} = L_2/l_\mathrm{lc}$, $E_\mathrm{lc} = L_2 l_\mathrm{lc}$ and $l_\mathrm{lc} = \sqrt{L_2/A}$. l_lc corresponds to the correlation length of the LC material, γ_lc and E_lc are the scale of the interfacial tension and of the energy, respectively. Eq.3.39 is the effective free energy of the membrane influenced by the LC material which is always in the equilibrium state in this case. From Eq.3.39, the coefficients of q^2 and q^4 correspond to the effective interfacial tension γ_eff and the effective bending rigidity K_eff of the membrane in our simulation, respectively,

$$\gamma_\mathrm{eff} = \gamma - \frac{\gamma_\mathrm{a}^2}{\gamma_\mathrm{lc}}, \tag{3.40}$$

$$K_\mathrm{eff} = K - \frac{K_\mathrm{a}^2}{E_\mathrm{lc}} - \frac{\gamma_\mathrm{a}}{\gamma_\mathrm{lc}}K_\mathrm{b}. \tag{3.41}$$

According to Eqs.3.40 and 3.41, $\gamma_{\rm eff}$ and $K_{\rm eff}$ are decreased by $\gamma_{\rm a}$ and $K_{\rm a}$ in the 2nd power of them respectively, which behaviors seem to correspond to our simulation results with respect to the anchoring parameter ξ. In addition, $K_{\rm eff}$ shows the different behavior from $\gamma_{\rm eff}$ due to the last term composed of $K_{\rm b}$. When $\gamma_{\rm a}$ is negative and $K_{\rm b}$ is positive (or, positive and negative, respectively), $K_{\rm eff}$ increases when $|K_{\rm a}^2/E_{\rm lc}| < (\gamma_{\rm a}K_{\rm b})/\gamma_{\rm lc}|$.

Here, we assume a dependence of $\gamma_{\rm a}$, $K_{\rm a}$, and $K_{\rm b}$ on the anchoring parameter ξ in our simulation model as following: $\gamma_{\rm a} = a(1-\xi)$, $K_{\rm a} = d_{\rm a}(1-\xi)$, and $K_{\rm b}$ is constant for ξ assumed above, where a and $d_{\rm a}$ are the constants without ξ dependence. In our simulation model, $\xi = 1$ corresponds to the isotropic interaction (the LC molecules interact with the spherical tail particles in an isotropic manner), while $\xi \neq 1$ gives an anisotropy for their interaction with an angle-dependent potential depth, which corresponds to the planar anchoring condition for $\xi < 1$ and to the homeotropic for $\xi > 1$, see Fig.2.2. We limit to $\xi \geq 1$, the homeotropic anchoring or the isotropic interaction. In above continuum model, $\gamma_{\rm a} < 0$ corresponds to the homeotropic anchoring, and no anchoring condition for $\gamma_{\rm a} = 0$. Then, we put above assumption for $\gamma_{\rm a} = a(1-\xi)$ (Using this assumption, we can realize the homeotropic condition $\gamma_{\rm a} < 0$ for $\xi > 1$ and the isotropic interaction $\gamma_{\rm a} = 0$ for $\xi = 1$.). For $K_{\rm a}$, we assumes the same form as $\gamma_{\rm a}$ because this term expresses the geometrical effect for the LC material to the membrane (due to the elastic coupling) and is strengthened by increasing the anchoring.

Next using above effective physical values, we try to fit these value to our simulation results.

3.3.2 Fitting for effective parameters

To investigate a parameter dependence for our simulation results of the interfacial tension and the bending rigidity shown in Sec.3.1, we conducted some independent simulations using other value for the GB parameter (the LC parameter in our simulation), κ'. Changing κ', the properties of the (pure) bulk LC material is changed, see Fig.3.10: (a) is the scalar order parameter S, (b) is the elastic constant L_2, (c) is the local energy density in terms of the LC ordering A. They are estimated for the same parameter set (the same energy, length parameters, temperature $T^* = 1.0$ and pressure $P^* = 3.0$. The number of particles is $N = 13500$.).

We conducted the simulations for 6 parameters, $\kappa' = 5.0, 8.0, 11.0, 14.0, 17.0, 20.0$ in the pure LC system as well as in the LC-confined system shown latter. S

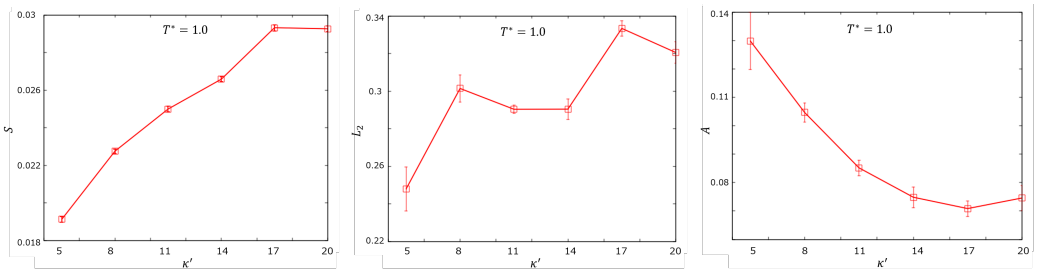

(a) **(b)** **(c)**

Fig. 3.10: The physical values in pure LC material at $T^* = 1.0$, $P^* = 3.0$, $N = 13500$, for different κ'. (a) the scalar order parameter, (b) the elastic constant, (c) the local energy density in terms of the LC ordering.

is calculated by the same way mentioned in Sec.3.1 (but no interface is in this case). L and A are estimated by the similar way to the estimation of γ_{eff} and K_{eff}. Since the LC material has an anisotropy (although it is in the weak nematic or the isotropic phase), we conduct the following operation for their estimaion according to [44]. We assumed that a spatial fluctuation of the tensor order parameter is weak for directions that are perpendicular to the main axis in the whole LC system (it corresponds to the eigenvector of the tensor order parameter with the maximum eigenbalue). Then we calculated the power spectrum of $Q_{xz}(\boldsymbol{q})$ and $Q_{yz}(\boldsymbol{Q})$ (z-direction corresponds to the main axis, and x,y are perpendicular to z, in this case), and fitted them using the following,

$$\langle|\tilde{Q}_{13}(\boldsymbol{q})|^2\rangle = \frac{k_{\text{B}}T}{V(2A + (L_1 + 2L_2)(q_x^2 + q_z^2))}, \tag{3.42}$$

$$\langle|\tilde{Q}_{23}(\boldsymbol{q})|^2\rangle = \frac{k_{\text{B}}T}{V(2A + 2L_2 q_x^2 + (L_1 + 2L_2)q_z^2)}. \tag{3.43}$$

In our simulation, since there is no external field, the accuracy is not good. However, the tendency of the LC properties for the increase in κ' can be obtained from Fig.3.10.

Using these values, we fitted for our simulation results in Sec.3.1 with respect to ξ using the dependence of γ_{a} and K_{a} on ξ and the constant K_{b} for ξ assumed in Sec.3.3.1 as seen in Fig.3.11; in Fig.3.11, a, b and c correspond to $\kappa' = 5.0, 14.0$ and 20.0, and 1 and 2 correspond to γ_{eff} and K_{eff}, respectively.

According to these figures, the behaviors of $\gamma_{\rm eff}$ and $K_{\rm eff}$ are almost similar to their modified forms in the continuum field theory, Eqs.3.40 and 3.41. The correspondence of fitting to $K_{\rm eff}$ seems to be bad, especially at the point on ξ with the maximal of $K_{\rm eff}$. This is because in such region with the deviation for fitting, since the orientation direction of the LC particles changes from the membrane normal to the planar direction along the membrane (see Fig.3.4 and Fig.3.6), the influence with the molecular level may appear. Again referring to our continuum model in Sec.3.3.1, we construct the effective free energy as considering the anchoring, mutual elastic coupling, and the effect of the rigidity of the nematic layer. The assumption that $K_{\rm b}$ is independet of the anchoring parameter ξ, we can realize the increasing behavior for $K_{\rm eff}$ in lower ξ region. Although the other effects may affect for the increasing behavior of $K_{\rm eff}$, we yet get them in this model.

From these fittings, of course including the cases of $\kappa' = 8.0, 11.0, 17.0$, we get the effective parameters as can be seen in Fig.3.12: (a) is a, (b) is $d_{\rm a}$, and (c) is $K_{\rm b}$, respectively, and they are plotted for L_2 of the elastic constant of the pure LC material. These L_2 values correspond to that for κ' using in the LC-confined system for each data points in Fig.3.12.

According to these figures, (i) a shows no dependence on L_2, (ii) $d_{\rm a}$ and $K_{\rm b}$ are the increasing function of L_2, although the accuracy is not good. Since a means the local coupling strength for the LC tensor order parametr to the membrane normal, it is valid that a is independent of the LC elastic constant L_2 which characterizes the correlation between the LC directors.

Figure 3.13 shows ξ giving the maximal of $K_{\rm eff}$ (defines it to $\xi_{\rm m}$). According to this figure, although $\xi_{\rm m}$ increases slightly at lower L_2 region, it is almost constant for larger L_2 region. Since the maximal of $K_{\rm eff}$ is realized by the competition between the elastic rigidity of the growed nematic layer and the effect of the anchoring. First increase in $K_{\rm eff}$ reflects stronger elasticity of the nematic layer (characterized by $K_{\rm b}$ in the continuum model) than the anchoring effect with respect to the elastic coupling (characterized by $K_{\rm a}$) and subsequently decreasing behavior is originated from the inversion between these contribution. Since both $K_{\rm a}$ and $K_{\rm b}$ are the increasing function of L_2 shown in (a) and (b) in Fig.3.12, respectively, these effects show similar strength for increasing the elasticity of the LC material L_2.

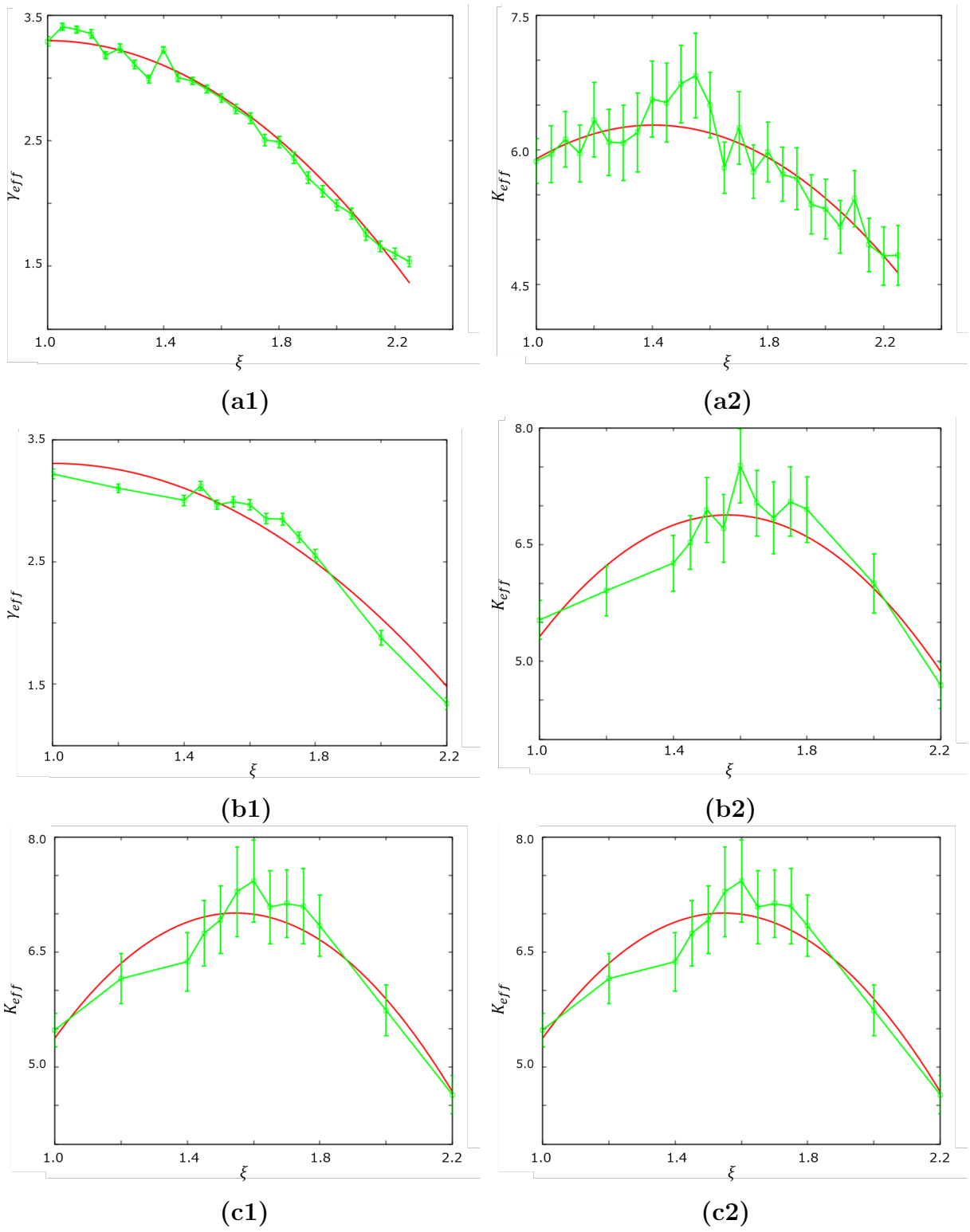

Fig. 3.11: The fitting pictures for $\kappa' = 5.0, 14.0, 20.0$ in the LC-confined system. The case $\kappa' = 5.0$ is the same as shown in Sec.3.1.

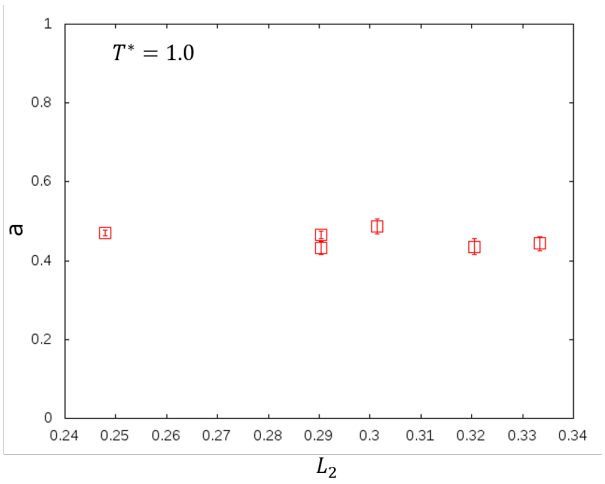

(a)

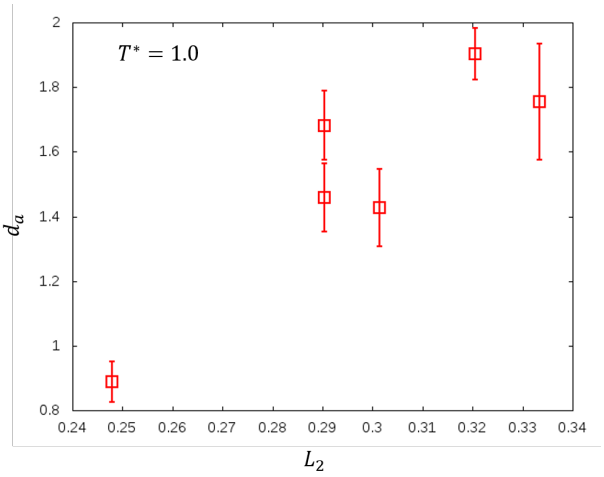

(b)

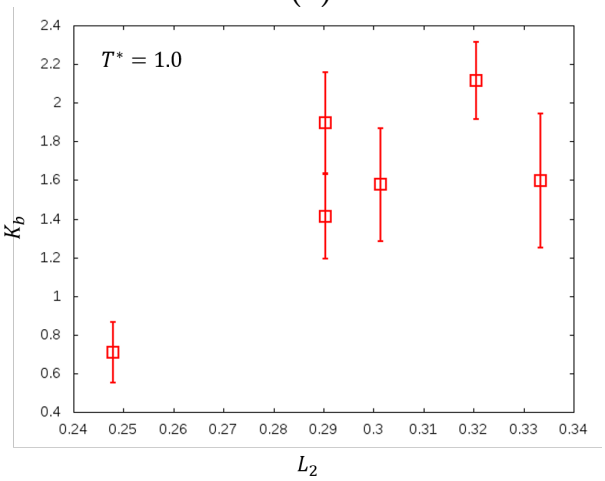

(c)

Fig. 3.12: The fitted effective parameters, (a) is a, (b) is d_{a}, and (c) is K_{b}, and they are plotted for L_2 of the elastic constant of the pure LC material for the corresponding κ'.

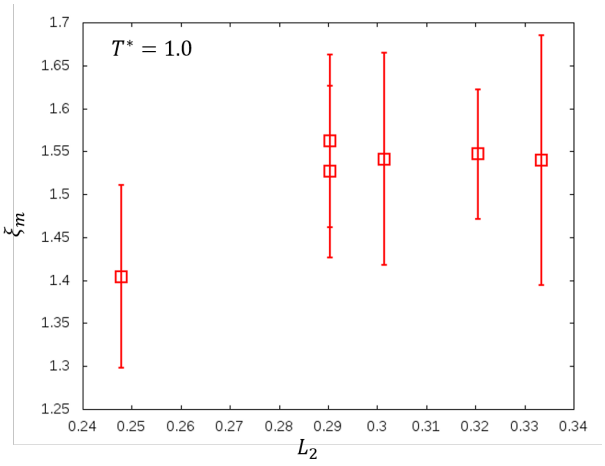

Fig. 3.13: The estimated ξ_{m} giving the maximal of K_{eff} for L_2.

Chapter 4

Conclusion

We conducted Monte-Carlo simulation of the membrane-confining LC system, and estimate the physical properties of the interface covered by the membrane and contacted with the LC material. We confirmed that the effective interfacial tension and the effective bending rigidity of the interface changes by changing the anchoring parameter for the LC material at the interface. Their changes also depend on the penetration of the confined particles and it is confirmed by the independent simulation for the oil-confined system, that is no anisotropy in the particles. However, the different behaviors are observed for the LC-confined system from the oil-confined system, then we considered the orientational properties-dependent interaction between the LC material and the membrane at interface. Then we first calculated the physical boundary conditions at such interface using the model free energy including the anchoring effect, and got the coupling between the membrane fluctuation and the LC orientational order and its gradient. Second we tried to construct the effective free energy including above physical boundary conditions as setting some coefficients, and got the effective forms of the interfacial tension and the bending rigidity of such system. Lastly we estimated these coefficients by fitting to our simulation results, and investigated their behavior for the elastic property of the LC material. According to these results, the constructed effective free energy has the reasonable form for our simulation system, at least.

Bibliography

[1] M. Toda, H. Matsuda, Y. Hiwatari, M. Wadachi; 「液体の構造と性質」, 岩波書店, 1976.

[2] P.G.de Gennes, J. Prost; *Oxford University Press: The Physics of Liquid Crystals*, 1993.

[3] L. Onsager; *Ann. N. Y. Acad. Sci.*, 1949, 51, 627.

[4] W. Maier, A. Z. Saupe; *Naturforsch.*, 1958, A13, 564; 1959, A14, 882; 1960, A15, 287.

[5] P. G. de Gennes; *Mol. Cryst. Liq. Cryst.*, 1971, 12, 193.

[6] F. C. Frank; *Discuss. Faraday Soc.*, 1958, 25, 19.

[7] P. Sheng; *Phys. Rev. A*, 1982, 26 1610.

[8] A. D. Rey, E. E. Herrera-Valencia; *Soft Matter*, 2014, 10, 1611.

[9] H. Stark, J. Fukuda, H. Yokoyama; *J. Phys. Cond. Matt.*, 2004, 16, 1911-1919.

[10] S. I. Hernandez, J. A. Moreno-Razo, A. Ramirez-Hernandez, E. Diaz-Herrera, J. P. Hernandez-Ortiz, J. J. de Pablo; *Soft Matter*, 2012, 8, 1443-1450.

[11] J. K. Gupta, J. S. Zimmerman, J. J. de Pablo, F. Caruso, N. L. Abbott; *Langmuir*, 2009, 25, 9016-9024.

[12] I. H. Lin, D. S. Miller, P. J. Bertics, C. J. Murphy, J. J. de Pablo, N. L. Abbott; *Science*, 2011, 332, 1297-1300.

[13] D. Hartono, C. Y. Xue, K. L. Yang, L. Y. L. Yung; *Adv. Funct. Mater.*, 2009, 19, 3574-3579.

[14] T. Bera, J. Deng, J. Fang; *J. Phys. Chem. B*, 2014, 118, 4970-4975.

[15] S. H. Yoon, K. C. Gupta, J. S. Borah, S. -Y. Park, Y. -K. Kim, J. -H. Lee, I. -K. Kang; *Langmuir*, 2014, 30, 10668-10677.

[16] L. N. Tan, N. L. Abbott; *J. Coll. Int. Sci.*, 2015, 449, 452-461.

[17] M. G. Tomilin, S. A. Povzon, A. F. Kurmashev, E. V. Gribanova, T. A. Efimova; *Liq. Cryst. Today*, 2001 10, 3.

[18] M. Khan, S.-Y. Park; *Sens. Act. B Chem.*, 2014, 202, 516-522.

[19] R. Rosso, M. C. P. Brunelli; *Continuum Mech. Thermodyn.*, 2001, 13, 383.

[20] E. C. Gartland, Jr., A. M. Sonnet, E. G. Virga; *Continuum Mech. Thermodyn.*, 2002, 14, 307.

[21] G. Ryskin, M. Kremenetsky; *Phys. Rev. Lett.*, 1991, 67, 1574.

[22] D. Svensek, S. Zumer; *Phys. Rev. Lett.*, 2003, 90, 155501.

[23] R. Stannarius, K. Harth; *Phys. Rev. Lett.*, 2016, 117, 157801.

[24] F. M. Leslie; *Q. J. Mechanics Appl. Math.*, 1966, 19, 357.

[25] C. Blanc, D. Svensek, S. Zumer, M. Nobili; *Phys. Rev. Lett.*, 2005, 95, 097802.

[26] L. Radzihovsky; *Phys. Rev. Lett.*, 2015, 115, 247801.

[27] J. Turk, D. Svensek; *Phys. Rev. E*, 2014, 89, 032508.

[28] T. Araki, H. Tanaka; *Phys. Rev. Lett.*, 2006, 97, 127801.

[29] T. Araki, F. Serra, H. Tanaka; *Soft Matter*, 2013, 9, 8107.

[30] [著] S. A. サフラン, [訳] 好村 滋行; コロイドの物理学 -表面・界面・膜面の熱統計力学-, 吉岡書店, 2001.

[31] U. Seifert; *Advances in Physics*, 1997, 46, 13-137.

[32] M. Matsumoto; 計量微分幾何学, 裳華房, 1975.

[33] X. Wang, Y.-Ki Kim, E. Bukusoglu, B. Zhang, D. S. Miller, N. L. Abbott; *Phys. Rev. Lett.*, 2016, 116, 147801.

[34] A. Bogi, P. Martinot-Lagarde, I. Dozov, M. Nobili; *Phys. Rev. Lett.*, 2002, 89, 225501.

[35] C. S. Park, N. A. Clark, R. D. Noble; *Phys. Rev. Lett.*, 1994, 72, 1838.

[36] I. I. Smalyukh, S. Chernyshuk, B. I. Lev, A. B. Nych, U. Ognysta, V. G. Nazarenko, O. D. Lavrentovich; *Phys. Rev. Lett.*, 2004, 93, 117801.

[37] J. Elgeti, F. Schmid; *Eur. Phys. J. E*, 2005, 18, 407-415.

[38] L. F. Rull, J. M. Romero-Enrique, A. Fernandez-Nieves; *J. Chem. Phys.*, 2012, 137, 034505.

[39] A. D. Rey; *Langmuir*, 2006, 22, 3491-3493.

[40] J. G. Gay, B. J. Berne; *J. Chem. Phys.*, 1981, 74(6), 3316-3319.

[41] R. Goetz, R. Lipowsky; *J. Chem. Phys.*, 1998, 108, 7397-7409.

[42] E. de Miguel, C. Vega; *J. Chem. Phys.*, 2002, 117, 6313-6322.

[43] J. C. Shillcock, R. Lipowsky; *J. Chem. Phys.*, 2002, 117, 5048-5061.

[44] M. P. Allen, M. A. Warren, M. R. Wilson, A. Sauron, W. Smith; *J. Chem, Phys.*, 1996, 105, 2850-2858.

Acknowledgement

This Doctor thesis is based on the study in Kawakatsu group belonging to the CMPT group at Tohoku University for 5 years, from Master course (2 years) to Doctor course (3 years). Through my research here, I would like to be profoundly grateful to Professor Kakawaktsu for his advising, discussions for my study, and his proofreading for my strange englich. Other group members discussed with me studiously, then I would also like to thank them.

Especially, I would like to thank my familly for their helping my 9 years in Tohoku University including the Bachelor course.